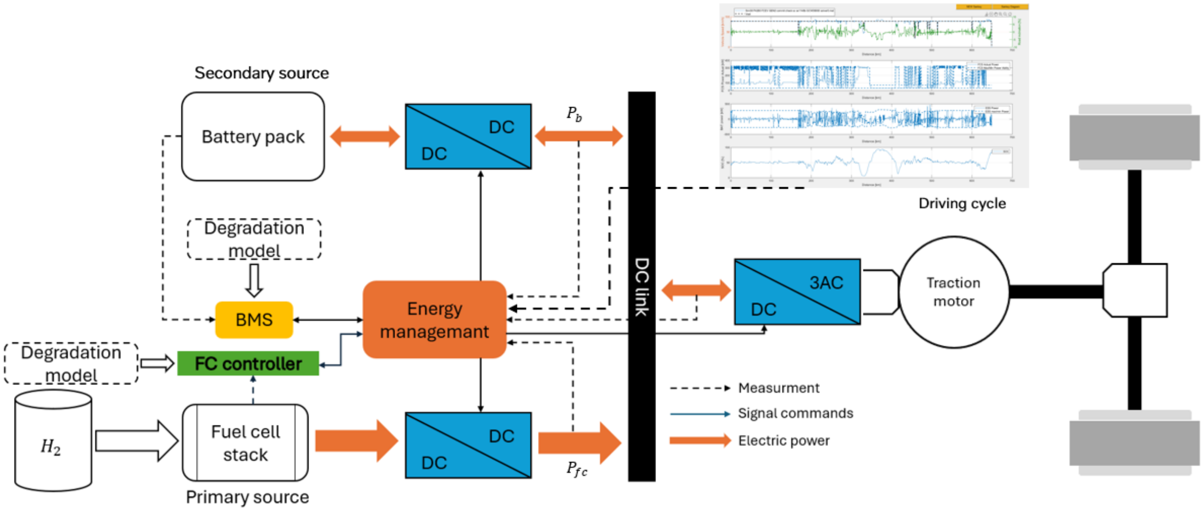

Health-Aware Equivalent Consumption Minimization Strategy for Fuel Cell Hybrid Electric Vehicles

Master's thesis in Systems, Control and Mechatronics

JIAYAO CHEN
ARVID LARSSON

DEPARTMENT OF ELECTRICAL ENGINEERING
CHALMERS UNIVERSITY OF TECHNOLOGY
Gothenburg, Sweden 2026
www.chalmers.se

Master's thesis 2026

Health-Aware Equivalent Consumption Minimization Strategy for Fuel Cell Hybrid Electric Vehicles

JIAYAO CHEN
ARVID LARSSON

Department of Electrical Engineering
Division of System Control
Chalmers University of Technology
Gothenburg, Sweden 2026

Health-Aware Equivalent Consumption Minimization Strategy for Fuel Cell Hybrid Electric Vehicles
JIAYAO CHEN
ARVID LARSSON

Supervisor: Tong Liu, Volvo Technology AB
Examiner: Torsten Wik, Electrical Engineering

Master's Thesis 2026
Department of Electrical Engineering
Division of System Control
Chalmers University of Technology
SE-412 96 Gothenburg
Telephone +46 31 772 1000

Cover: Schematic illustration of an FCHEV powertrain with an enhanced, health-conscious ECMS controller for real-time energy management, highlighting battery and fuel-cell aging considerations.

Typeset in LaTeX
Printed by Chalmers Reproservice
Gothenburg, Sweden 2026

Health-Aware Equivalent Consumption Minimization Strategy for Fuel Cell Hybrid Electric Vehicles
JIAYAO CHEN
ARVID LARSSON
Department of Electrical Engineering
Chalmers University of Technology

Abstract

Fuel cell hybrid electric vehicles (FCHEVs) are gaining increasing attention as the transition toward sustainable mobility accelerates. One of the key challenges in the application of FCHEVs is to achieve an optimal power split between the fuel cell and the battery. Traditional energy management strategies mainly focus on minimizing energy consumption. However, from a life-cycle perspective, the degradation of system components also has a significant impact on overall efficiency.

This thesis proposes a health-aware equivalent consumption minimization strategy that considers both fuel consumption and component degradation. The degradation related costs are incorporated into the traditional cost function, which otherwise accounts only for hydrogen consumption. An analytical solution is then developed to obtain the optimal solution for the control problem. To reduce the computational complexity and make the cost function differentiable, Taylor expansion is employed and the cost function is reformulated as a piecewise quadratic function.

The proposed method is implemented and evaluated within Volvo's Global Simulation Platform, enabling system-level validation under representative driving conditions. The simulation results show that the proposed method can significantly mitigate fuel cell degradation, with an acceptable increase in battery degradation and fuel consumption. Meanwhile, the charge sustaining performance and drivability are largely preserved.

Keywords: fuel cell hybrid electric vehicles, equivalent consumption minimization strategy, degradation, health-aware.

Acknowledgements

We would like to express our sincere gratitude to our examiner, Torsten Wik, and our supervisor, Tong Liu, for their insightful guidance and continuous support throughout the thesis work.

Our appreciation also goes to Behrooz Razaznejad at Volvo Group for providing us with the opportunity and the necessary resources to carry out this research.

Finally, we are grateful to our families, friends, and colleagues at Volvo Group for their encouragement and help.

Jiayao Chen and Arvid Larsson, Gothenburg, June 2026

List of Acronyms

Below is the list of acronyms that have been used throughout this thesis listed in alphabetical order:

ECMS	Equivalent Consumption Minimization Strategy
EMS	Energy Management System
ESS	Energy Storage System
FCHEV	Fuel Cell Hybrid Electric vehicle
FCS	Fuel Cell System
GSP	Global Simulation Platform
HEV	Hybrid Electric vehicle
HIL	Hardware-in-the-Loop
MIL	Model-in-the-Loop
PMP	Pontryagin's Minimum Principle
SIL	Software-in-the-Loop
SOC	State of Charge

Nomenclature

Below is the nomenclature of indices, sets, parameters, and variables that have been used throughout this thesis.

Indices

i	Indices for fuel cell working conditions
t	Index for time step

Sets

$\mathbf{G}$	Set of m inequalities
U	Set of admissible control values
Ω	Set of admissible states

Parameters

t_f	Length of trip
t_0	Starting time
x_{target}	State target
m	Number of inputs
n	Number of states
p	Number of controls
K	Constraint penalty parameter
λ_0	Initial guess of co-state vector
SOC_{target}	Target SOC value
SOC_{min}	Minimum SOC value
SOC_{max}	Maximum SOC value

$P_{bat,min}$	Minimum battery power
$P_{bat,max}$	Maximum battery power
$V_{oc,nom}$	Nominal open circuit voltage
Q_{nom}	Nominal charge capacity
η_{coul}	Coulombic efficiency
Q_{lhv}	Lower heating value
a	Penalty shaping exponent
$\xi_{start-stop}$	Degradation rate for start-stop
ξ_{low}	Degradation rate under low load
ξ_{high}	Degradation rate under high load
ξ_{change}	Degradation rate under load change
c_{fc}	Price of fuel cell system
ΔV_{fc}	Allowable voltage drop
N_{fc}	Number of fuel cells in the stack
b	Pre-exponential factor
c	C-rate
R	Ideal gas constant
z	Power-law factor
c_{bat}	Price of the battery
c_{H_2}	Cost of hydrogen

Variables

$\dot{m}_f$	Mass flow rate of fuel
u	Control input
x	State variable
P_{bat}	Battery output power
T	Motor torque
ω	Motor speed
λ	Co-state vector
P_{req}	Power request from driver
E_{ech}	Electrochemical energy variation
P_{fuel}	Fuel power
P_{ech}	Battery electrochemical power

V_{oc}	Open circuit voltage
I	Battery current
P_{eng}	Engine power
η_{eng}	Engine efficiency
η_{bat}	Battery efficiency
$\dot{m}_{ress}$	Virtual fuel consumption
s_{eq}	Virtual specific fuel consumption
s	Equivalence factor
s_{chg}	Equivalence factor in charge case
s_{dis}	Equivalence factor in discharge case
p	SOC deviation
C_{fc}	Degradation cost of fuel cell
$C_{start-stop}$	Degradation cost of fuel cell induced by fuel cell start-stop
C_{low}	Degradation cost of fuel cell induced by low working load
C_{high}	Degradation cost of fuel cell induced by high working load
C_{change}	Degradation cost of fuel cell induced by working load changes
C_{bat}	Degradation cost of battery
T_{low}	Duration of fuel cell in low load
T_{high}	Duration of fuel cell in high load
$N_{start-stop}$	Number of start stop cycles
T_a	Battery temperature
A	Ampere-hour throughput
E_a	Activation energy
A_{EOL}	Total throughput throughout the battery lifetime
N_{EOL}	Total number of cycles throughout the battery lifetime
P_{H_2}	Hydrogen power
P_{fc}	Fuel cell output power
P_b	Electricity power

Contents

List of Figures

List of Tables

1
Introduction

The demand for converting and generating energy is a human necessity. Fossil fuels are a common source for fulfilling this demand. One of the biggest challenges associated with fossil fuels is climate change caused by their combustion. Furthermore, fossil fuel resources are finite and non-renewable, whereas global energy demand continues to increase with the development of modern society. These issues highlight the need for sustainable and inexhaustible energy alternatives.

As vehicles are one of the largest consumers of fossil fuels, the automotive industry is undergoing a rapid transition toward sustainable powertrain solutions in recent years. Batteries and fuel cells are two key components that are increasingly used in this transition process [1][2].

While batteries and fuel cells offer significant benefits in reducing carbon emissions, they also have inherent drawbacks. For battery electric vehicles, driving range remains a key concern for consumers [3][4]. In addition, the relatively long charging time further increases range anxiety [5]. But increasing energy density relies on advances in battery technology; however, higher energy density is often associated with increased safety risks and higher costs, resulting in a complex trade-off between performance, cost, and safety [6][7].

A fuel cell is an electrochemical device that converts chemical energy into electrical energy. Fuel cells and batteries share a similar structural configuration, consisting of anode, cathode, and electrolyte. However, unlike batteries, where reactants are stored internally, a typical proton exchange membrane fuel cell operates continuously with hydrogen supplied to the anode and oxygen to the cathode. The membrane allows only protons to pass through while forcing electrons to flow through an external circuit, thereby generating current. In addition, platinum-based catalysts are typically used to accelerate the reaction, which increases the system cost of the fuel cell [8][9].

With the development of hydrogen refueling infrastructure, range anxiety in fuel cell vehicles can be mitigated. However, due to limitations in gas transport dynamics, fuel cells exhibit relatively slow transient responses [10][11]. As a result, integrating a battery as an energy buffer becomes necessary. Such fuel cell hybrid electric vehicles (FCHEVs) are attracting increasing attention in both research and industry.

1.1 Background

FCHEVs use fuel cells as the main power source and batteries as an auxiliary device that stores regenerated energy and provides peak power [12]. Fuel cells are most efficient at partial load and operate best under stable conditions [13], whereas the battery can supply high current to compensate for the fuel cell's dynamic limitations.

To obtain an optimal power split between fuel cells and batteries under different driving conditions, an energy management strategy is essential. Existing energy management systems (EMSs) can be mainly divided into rule-based and optimization-based EMSs [14]. Rule-based EMSs are designed based on human expertise and rely on identifying efficient operating points. Generally, rule-based EMSs are easy to implement in real-time applications, but achieving optimal performance is difficult [12]. Optimization-based EMSs can be further divided into global and real-time optimization strategies. Global optimization strategies obtain optimal solutions by solving for a cost function over a known driving cycle, whereas real-time strategies operate based on instantaneous or predicted driving conditions.

Due to increasing requirements in real FCHEV applications, existing EMS functionalities need to be further refined and enhanced. Traditional approaches mainly focus on minimizing energy consumption and often overlook long-term component degradation. From a life-cycle perspective, improving system durability also plays an important role in enhancing overall efficiency [15]. Therefore, a central challenge in this field is the development of energy management strategies that optimize both fuel economy and the longevity of key components, such as fuel cells and batteries.

Energy efficiency should not be regarded as the sole optimization objective; the lifespans of powertrain components—particularly the fuel cell system (FCS) and energy storage system (ESS)—must be preserved. Additionally, the charge sustainability of the ESS, typically measured by the state of charge (SOC), should be maintained within an appropriate range to ensure reliable operation [16]. Furthermore, decoupling transient power flows between the FCS and ESS provides greater flexibility for optimization, enabling more balanced performance outcomes.

1.2 Literature review

Managing energy in a hybrid vehicle involves deciding, at each instant, the amount of power drawn from each energy source [17]. Control of a hybrid vehicle can be divided into two levels: component-level control and supervisory control. Component-level control governs elements such as the engine, electric motor, generator, transmission, and brakes, ensuring accurate and safe operation. In contrast, supervisory control—also referred to as the EMS—determines how energy should be used at each moment. For example, it decides how power is split between the fuel cell and battery, minimizes fuel consumption, and maintains the battery SOC within a safe range.

To address the energy management problem mentioned in Section 1.1, various health-aware strategies have been developed. Based on their decision-making mechanisms, these strategies can be classified into rule-based, optimization-based, and learning-based approaches.

1.2.1 Rule-based strategies

Rule-based strategies are among the most commonly used approaches in hybrid vehicle applications. These strategies rely on predefined control rules to determine the control action at each instant [18]. The rules are typically derived from engineering experience rather than explicit optimization [19]. Examples include using the primary energy source when the battery SOC falls below a lower threshold, and enabling pure electric mode when the SOC exceeds an upper threshold.

Overall, rule-based strategies are easy to implement [20], and their low computational burden makes them suitable for real-time control. However, defining effective rules and thresholds is challenging, and the resulting solution is likely not optimal.

1.2.2 Optimization-based strategies

Optimization-based strategies formulate the energy management problem as an optimization problem, minimizing a predefined cost function where system dynamics and constraints are incorporated into the model.

These strategies can be divided into offline and online methods. Offline methods, such as dynamic programming, can provide globally optimal solutions. However, they require prior knowledge of the entire driving cycle, making them unsuitable for real-time implementation. In addition, their high computational complexity leads to time-consuming calculations [21].

To meet real-time requirements, various online optimization methods have been developed. Among them, Pontryagin's Minimum Principle (PMP) and the Equivalent Consumption Minimization Strategy (ECMS), which can be regarded as a realization of PMP, are among the most important approaches [17]. These methods transform the global optimization problem into a local one by minimizing an instantaneous cost function, and they have been widely applied in hybrid vehicle applications.

ECMS is a commonly used approach for real-time energy management in FCHEVs [22]. By means of an equivalence factor, traditional ECMS minimizes the equivalent energy consumption, defined as the sum of actual hydrogen consumption by the FCS and the equivalent electrical energy consumption of the ESS. By adding degradation related factors into the cost function, ECMS can be adapted to health-aware ECMS.

A detailed introduction to PMP and ECMS theory will be provided in Chapter 2.

1.2.3 Learning-based strategies

In contrast to rule-based and optimization-based strategies, learning-based approaches do not rely on explicit system models or expert knowledge. Instead, machine learning techniques are used to learn and adapt energy management strategies based on historical and real-time data [23]. Common approaches include reinforcement learning, clustering methods, and neural network-based techniques.

At present, learning-based strategies remain challenging to implement in real-world vehicle applications. Constructing effective datasets is time-consuming [24], and training models requires significant computational resources. Consequently, their application in hybrid vehicles is still limited.

1.2.4 Existing solutions

Sahwal et al. [25] propose an Advanced ECMS that reformulates the cost function. The novel cost function includes a modified equivalence factor accounting for multiple health-critical factors: battery and fuel cell temperature, degradation of fuel cell due to low power and high power operation, number of starts and stops of fuel cell, and transient loading. Furthermore, a fuzzy logic controller is developed to adaptively vary the weights for each sub-component during run time, thereby increasing or decreasing the component's importance during optimization. Simulation results show that both at urban and highway driving conditions, Advanced ECMS presents better performance at reducing fuel consumption and degradation.

In [26], Jia et al. propose a learning-based model predictive (L-MPC) energy management system for a fuel cell hybrid electric bus with health awareness. The proposed L-MPC system performs better than MPC over long prediction horizons. When compared to a reinforcement learning algorithm called TD3, L-MPC was very effective in saving hydrogen fuel consumption, slowing down battery aging and reducing fuel cell degradation. L-MPC could also, when compared to MPC and TD3, save on hydrogen cost, battery use cost and total operating cost.

1.3 Purpose

This thesis was conducted in collaboration with Volvo Group. The ECMS framework developed by Volvo Group serves as the basis for the work presented in this thesis.

The aim of the thesis project is to study enhanced ECMS for real-time energy management in FCHEVs. The objective is to critically evaluate existing health-conscious and adaptive ECMS-based approaches, benchmark their performance, and explore innovative enhancements. Emphasis will be placed on strategies that address not only fuel consumption but also the health and degradation of energy sources.

1.4 Research questions

The research questions posed for this thesis are as follows:

- How can the ECMS framework be reformulated to incorporate degradation effects in fuel cell hybrid vehicles?

- Can the resulting non-linear and non-differentiable optimization problem be solved analytically for real-time implementation, and if so, how?
- What impact does the proposed health-aware strategy have on energy efficiency and degradation compared to conventional ECMS methods?

1.5 Limitations

The basic verification method for this research is model-based simulation, and experimental validation is outside the scope of the thesis. Also, the model used for simulation is based on Volvo's Global Simulation Platform (GSP). Detailed electrochemical degradation mechanism of FCS and ESS is not explicitly modeled.

As mentioned in Section 1.2 there are already multiple different existing health-conscious EMSs. This thesis focuses mainly on real-time optimization strategies, particularly ECMS solutions.

This thesis focuses on real-time power or torque split between FCS and ESS. Future speed or torque demand prediction is not considered in the energy management process. As a result, the strategy may be less effective at saving hydrogen consumption and reducing degradation than prediction-based energy management strategies.

2
Theory

This chapter presents the necessary theory for understanding energy management strategies investigated in this thesis. First, the fundamental principles of a fuel cell hybrid vehicle are introduced, followed by a review of energy management strategies, with focus on ECMS. The chapter ends with relevant concepts within component degradation.

2.1 The optimal control problem

In general, the energy management problem in a hybrid vehicle can be formulated as a finite-horizon optimization problem [17]. Its solution can be obtained using optimal control theory techniques, which aim to determine a control law that optimizes a specified performance criterion, typically expressed as an integral cost function over the considered time interval.

A general optimal energy management problem in a hybrid electric vehicle can be formulated as

$$J = \int_{t_0}^{t_f} \dot{m}_f(\mathbf{u}(t), t)dt, \tag{2.1}$$

where $\dot{m}_f$ is the mass flow rate of fuel in [g/s], t_f is the length of the trip, $t_0 = 0$ is the starting time [17]. The integral J is minimized so that the optimal control input $u(t)$ can be found, which is equivalent to minimizing the fuel consumption $\dot{m}_f$. From system dynamics with $x(t) = SOC$ and $u(t) = P_{bat}$ (battery power) the following general formula is given

$$\dot{x} = f(x(t), u(t)). \tag{2.2}$$

This general optimization problem is subject to both local (instantaneous) and global (integral) constraints. A global constraint is that the final SOC value $x(t_f)$ should reach a predefined target x_{target}

$$x(t_f) = x_{target}, \tag{2.3}$$

or

$$x(t_f) - x_{target} = \Delta x = 0. \tag{2.4}$$

As mentioned, there are also local constraints on both the state and control variables. The constraints on the states make sure that the SOC remains within a certain maximum and minimum value. On the other hand, local constraints on the control variables make sure that the physical operation limits are met. Generally the local constraints are

$$\begin{aligned} SOC_{min} &\leq SOC \leq SOC_{max} \\ P_{bat,min} &\leq P_{bat} \leq P_{bat,max} \\ T_{x,min} &\leq T_x \leq T_{x,max} \\ \omega_{x,min} &\leq \omega_x \leq \omega_{x,max} \end{aligned} \tag{2.5}$$

where the two last ones are the limit on the motor torque and motor speed. Finally the optimal control problem is to find the optimal control u^* such that the cost function (2.1) is minimized and the constraints in (2.2), (2.3) and (2.5) are met.

The optimal control problem can also be formulated using soft rather than hard constraints on the final target value $x(t_f)$, using the system dynamics as in (2.2), but with the following performance measure instead

$$J = \phi(\mathbf{x}(t_f)) + \int_{t_0}^{t_f} \dot{m}_f(\mathbf{u}(t), t)dt, \tag{2.6}$$

where $\phi(\mathbf{x}(t_f))$ is a penalty function, the function of which is to bring the final value as close as possible to the target value. The performance index (2.6) can be written more generally as

$$J = \phi(\mathbf{x}(t_f)) + \int_{t_0}^{t_f} L(\mathbf{x}(t), \mathbf{u}(t), t)dt, \tag{2.7}$$

where L is a the cost function, in which several objectives can be combined. For instance fuel consumption and battery aging. The optimal control problem in this case, is choosing the control input $\mathbf{u} : [t_0, t_f] \mapsto \mathbb{R}^p$ so that (2.7) is minimized under dynamic, local, and global constraints. The constraints on the states can be generally expressed as the set of admissible states were $\mathbf{G}(\mathbf{x}, t) \leq 0$ hold, i.e.

$$\Omega_{\mathbf{x}}(t) = \{\mathbf{x} \in \mathbb{X}^{\ltimes} | \mathbf{G}(\mathbf{x}, t) \leq 0\}, \tag{2.8}$$

with $\mathbf{G}(\mathbf{x}, t) : \mathbb{R}^{n+1} \mapsto \mathbb{R}^m$ being the set of m inequalities that the state vector must satisfy. Both the admissible states and controls are then defined as

$$\begin{cases} \mathbf{x}(t) \in \Omega_{\mathbf{x}}(t) \\ \mathbf{u}(t) \in U(t), \end{cases} \qquad \forall t \in [t_0, t_f] \tag{2.9}$$

where $U(t)$ is the set of admissible control values at time t. Finding the optimal control $\mathbf{u}^*$ such that (2.7) is minimized, and (2.2) and (2.9) are satisfied is called the constrained finite time-horizon optimal control problem.

2.2 Solving the optimal control problem

In the following chapters, different methods for solving the optimal control problem will be presented and discussed.

2.2.1 Pontryagin's Minimum Principle

Pontryagin's Minimum Principle (PMP) forms a set of necessary optimality conditions [17]. Any control law $\mathbf{u}(t)$ that satisfies these conditions is referred to as an extremal. Since the minimum principle establishes only necessary conditions, any optimal solution, when it exists, must correspond to an extremal control; however, not every extremal control is optimal.

For the constrained finite time-horizon optimal control problem discussed in Section 2.1, the Hamiltonian is the scalar

$$H(\mathbf{x}(t), \mathbf{u}(t), \boldsymbol{\lambda}(t), t) = L(\mathbf{x}(t), \mathbf{u}(t), t) + \boldsymbol{\lambda}(t)^\top \cdot f(\mathbf{x}(t), \mathbf{u}(t), t), \tag{2.10}$$

where $f(\mathbf{x}(t), \mathbf{u}(t), t)$ is the system dynamics, $L(\mathbf{x}(t), \mathbf{u}(t), t)$ is the cost and $\boldsymbol{\lambda}(t)$ is the vector of optimization variables, or co-states, having the same dimension as $\mathbf{x}(t)$. According to PMP, if $\mathbf{u}^*$ is the optimal control law for the constrained finite time-horizon optimal control problem, then the following conditions are satisfied:

1. States and co-states:

$$\dot{\mathbf{x}}^*(t) = \left.\frac{\partial H}{\partial \boldsymbol{\lambda}}\right|_{\mathbf{u}^*(t)} = f(\mathbf{x}^*(t), \mathbf{u}^*(t), t) \tag{2.11}$$

$$\begin{aligned}\dot{\boldsymbol{\lambda}}^*(t) &= -\left.\frac{\partial H}{\partial \mathbf{x}}\right|_{\mathbf{u}^*(t)} = h(\mathbf{x}^*(t), \mathbf{u}^*(t), \boldsymbol{\lambda}^*(t), t) = \\ &= -\frac{\partial L}{\partial \mathbf{x}}(\mathbf{x}^*(t), \mathbf{u}^*(t), t) - \boldsymbol{\lambda}^*(t) \cdot \left[\frac{\partial f}{\partial \mathbf{x}}(\mathbf{x}^*(t), \mathbf{u}^*(t), t)\right]^\top\end{aligned} \tag{2.12}$$

$$\mathbf{x}^*(t_0) = x_0 \tag{2.13}$$

$$\mathbf{x}^*(t_f) = x_{target} \tag{2.14}$$

2. $\mathbf{u}^*(t)$ globally minimizes the Hamiltonian:

$$H(\mathbf{u}(t), \mathbf{x}^*(t), \boldsymbol{\lambda}^*(t), t) \geq H(\mathbf{u}^*(t), \mathbf{x}^*(t), \boldsymbol{\lambda}^*(t), t) \quad \forall \mathbf{u}(t) \in U(t), \forall t \in [t_0, t_f], \tag{2.15}$$

or in other words the optimal solution $\mathbf{u}^*(t)$ is

$$\mathbf{u}^*(t) = \arg \min_{\mathbf{u}(t) \in U(t)} H(\mathbf{u}(t), \mathbf{x}(t), \boldsymbol{\lambda}(t), t). \tag{2.16}$$

To also guarantee that the states respect local constraints and are within $\Omega_{\mathbf{x}}(t)$ at any given time instance, an extra cost is added to the Hamiltonian, which is

activated whenever the constraints are reached or crossed. The local constraints are violated when
1. the state value is above its upper limit

$$G_1(\mathbf{x}(t) = \mathbf{x}(t) - \mathbf{x}_{max} > 0 \tag{2.17}$$

2. or, when the state value is below its lower limit

$$G_2(\mathbf{x}(t)) = \mathbf{x}_{min} - \mathbf{x(t)} > 0. \tag{2.18}$$

To prevent this the following constraint is introduced

$$\mathbf{G}^{(1)}(\mathbf{x}(t), \mathbf{u}(t), t) = \begin{cases} G_1^1(\mathbf{x}(t), \mathbf{u}(t), t) = \dfrac{dG_1}{dt} = \dot{\mathbf{x}}(t) = f(\mathbf{x}(t), \mathbf{u}(t), t) \\ G_2^1(\mathbf{x}(t), \mathbf{u}(t), t) = \dfrac{dG_2}{dt} = -\dot{\mathbf{x}}(t) = -f(\mathbf{x}(t), \mathbf{u}(t), t), \end{cases} \tag{2.19}$$

the new Hamiltonian is then

$$\begin{aligned} H(\mathbf{x}(t), \mathbf{u}(t), \boldsymbol{\lambda}(t), t) &= L(\mathbf{x}(t), \mathbf{u}(t), t) + \boldsymbol{\lambda}(t)^\top f(\mathbf{x}(t), \mathbf{u}(t), t) + \\ &\quad + w(\mathbf{x})^\top f(\mathbf{x}(t), \mathbf{u}(t), t) \\ &= L(\mathbf{x}(t), \mathbf{u}(t), t) + \left(\boldsymbol{\lambda}(t)^\top + w(\mathbf{x})^\top\right) f(\mathbf{x}(t), \mathbf{u}(t), t) \end{aligned} \tag{2.20}$$

with $w(\mathbf{x})$ being

$$w(\mathbf{x}) = \begin{cases} 0 & \mathbf{G}(\mathbf{x}(t)) < 0 \\ -K & G_1(\mathbf{x}(t)) \geq 0 \\ K & G_2(\mathbf{x}(t)) \geq 0, \end{cases} \tag{2.21}$$

where the value of K is arbitrary. The co-state function (2.13) can also be modified because of the new Hamiltonian (2.20):

$$\dot{\boldsymbol{\lambda}}^*(t) = -\frac{\partial L}{\partial \mathbf{x}}(\mathbf{x}^*(t), \mathbf{u}^*(t), t) - (\boldsymbol{\lambda}^*(t) + w(\mathbf{x})) \cdot \left[\frac{\partial f}{\partial \mathbf{x}}(\mathbf{x}^*(t), \mathbf{u}^*(t), t)\right]^\top. \tag{2.22}$$

In the specific case of a hybrid electric vehicle (HEV) the number of states and controls are $n = 1$ and $p = 1$, respectively [17]. The state $x = SOC$ must be within SOC_{min} and SOC_{max}, i.e. the set of admissible states is $\Omega_{SOC}(t) = [SOC_{min}, SOC_{max}]$. For the control input $u = P_{bat}(t)$, the set of admissible controls are $U_{P_{bat}}(t) = [P_{bat,min}(t), P_{bat,max}(t)]$. The Hamiltonian for the HEV energy management problem is therefore:

$$H(SOC(t), P_{bat}(t), \lambda(t), P_{req}(t)) = \dot{m}_f(P_{bat}(t), P_{req}(t)) + (\lambda(t) + w(SOC)) \cdot \dot{SOC}(t), \tag{2.23}$$

with P_{req} being the power request from the driver. The necessary conditions are as follows:

$$P^*_{bat}(t) = \arg \min_{P_{bat}(t) \in U_{P_{bat}}(t)} H(P_{bat}(t), SOC(t), \lambda(t), P_{req}(t)) \tag{2.24}$$

$$\dot{SOC}^*(t) = f(SOC^*(t), P^*_{bat}(t)) \tag{2.25}$$

$$\begin{aligned} \dot{\lambda}^*(t) &= -(\lambda^*(t) + w(SOC))\frac{\partial f}{\partial SOC}(SOC^*(t), P^*_{bat}(t)) \\ &= h(SOC^*(t), P^*_{bat}(t), \lambda^*(t)) \end{aligned} \tag{2.26}$$

$$SOC^*(t_0) = SOC_0 \tag{2.27}$$

$$SOC^*(t_f) = SOC_{target} \tag{2.28}$$

The shooting method for obtaining the necessary conditions for PMP generally starts with an initial guess of the co-state λ_0 and the PMP conditions are solved over the optimization horizon $[t_0, t_f]$. The obtained value at the end of the simulation $SOC(t_f)$ is then compared to the desired one SOC_{target}. If $SOC(t_f) - SOC_{target} < 0$ the initial co-state λ_0 is increased, if $SOC(t_f) - SOC_{target} > 0$ the initial co-state λ_0 is decreased or if the obtained value reaches the target the algorithm is ended.

Then, the implementation of the necessary PMP conditions, starts with, given a power request P_{req}, at each instant of time over the optimization horizon $[t_0, t_f]$, the Hamiltonian is formulated and minimized. From this the optimal control P^*_{bat} is generated and then applied. Then state and co-state derivative is calculated.

The PMP formulation can be reformulated with the electrochemical energy derivative $E_{ech}(t)$ as the system state instead of SOC, and the power equivalent to the fuel flow rate, P_{fuel}, instead of the fuel mass flow rate $\dot{m}_f(t)$. The electrochemical energy variation $E_{ech}(t)$ is defined as

$$E_{ech}(t) = \int_{t_0}^{t} P_{ech}(t) = \int_{t_0}^{t} V_{oc}(SOC)I(t)dt, \tag{2.29}$$

where P_{ech} is battery electrochemical power, V_{oc} is the open cicuit voltage and I is the battery current. In a charge-sustaining HEV, the following is assumed: $V_{oc} \approx const = V_{oc,nom}$. The electrochemical energy variation $E_{ech}(t)$ is then

$$E_{ech}(t) = V_{oc,nom} \int_{t_0}^{t} I(t)dt = V_{oc,nom} \cdot Q_{nom} \cdot \eta_{coul} \cdot (SOC(t_0) - SOC(t)), \tag{2.30}$$

where Q_{nom} is the nominal charge capacity and η_{coul} is the Coulombic efficiency. The power equivalent to the fuel flow rate P_{fuel} is:

$$P_{fuel}(t) = Q_{lhv}\dot{m}_f(t), \tag{2.31}$$

where Q_{lhv} is fuel lower heating value (MJ/kg). Then taking the derivative of The electrochemical energy variation $E_{ech}(t)$ with respect to time gives:

$$P_{ech}(t) = \dot{E}_{ech}(t) = -S\dot{O}C(t)V_{oc,nom}Q_{nom}\eta_{coul} = V_{oc,nom}I(t). \tag{2.32}$$

The Hamiltonian is

$$H = P_{fuel}(t) + \lambda(t) \cdot P_{ech}(t), \tag{2.33}$$

or with the extra cost:

$$H = P_{fuel}(t) + (\lambda(t) + w(SOC)) \cdot P_{ech}(t). \tag{2.34}$$

The co-state $\lambda(t)$ also changes to:

$$\dot{\boldsymbol{\lambda}}^{*}(t) = -\frac{\partial H}{\partial E_{ech}} = -(\lambda^{*}(t) + w(SOC))\frac{\partial P_{ech}}{\partial E_{ech}}. \tag{2.35}$$

2.2.2 Equivalent Consumption Minimization Strategy

In charge-sustaining HEV's the difference between the initial and final battery SOC over a drive cycle is negligible, i.e. $SOC(t_f) \approx SOC_{target}$ [17]. Therefore, all energy is generated from the fuel and the battery only acts as an energy buffer. Any electrical energy discharged from the battery must be replenished. During any given point in time the battery power can be positive (discharge case) or negative (charge case). In the discharge case the battery must be recharged at some time in the future. How much fuel it takes depends on operating condition of the engine at the time and how much energy can be recovered from regenerative braking. On the other hand, during the charge case, the stored energy is used to elevate the engine load, meaning that the engine does not need as much power or torque and therefore fuel is saved. This again depends on the operating condition of the engine.

The basic principle of ECMS is that the electrical energy is assigned a cost, in which the use of stored electrical energy is equivalent to using or saving fuel. Accordingly, in both battery charging and discharging modes, an equivalent or virtual fuel consumption $\dot{m}_{ress}(t)$ (g/s) can be associated with the electrical energy flow and added to the instantaneous fuel mass flow rate $\dot{m}_f$ (g/s) to obtain an instantaneous equivalent fuel consumption to be minimized $\dot{m}_{f,eqv}(t)$:

$$\dot{m}_{f,eqv}(t) = \dot{m}_f + \dot{m}_{ress}(t), \tag{2.36}$$

where the instantaneous fuel consumption $\dot{m}_f$ is:

$$\dot{m}_f = \frac{P_{eng}(t)}{\eta_{eng}(t)Q_{lhv}}, \tag{2.37}$$

with $\eta_{eng}(t)$ being the engine efficiency and P_{eng} is engine power. The virtual fuel consumption $\dot{m}_{ress}(t)$ is:

$$\dot{m}_{ress}(t) = s_{eq}(t) \cdot P_{bat}(t), \tag{2.38}$$

where $s_{eq}(t)$ is the virtual specific fuel consumption (g/kWh). The virtual specific fuel consumption is proportional to an equivalence factor $s(t)$ that changes with respect to if the battery is being charged or discharged:

$$\dot{m}_{ress}(t) = \frac{s(t)}{Q_{lhv}} P_{bat}(t). \tag{2.39}$$

The equivalence factor $s(t)$ is defined separately for battery charging and discharging modes, denoted as $s_{chg}(t)$ and $s_{dis}(t)$, respectively. The operating mode is determined by the sign of the battery power $P_{bat}(t)$: $P_{bat}(t) > 0$ indicates battery discharging, whereas $P_{bat}(t) < 0$ indicates battery charging. Accordingly, $s(t)$ is defined as

$$s(t) = \begin{cases} s_{dis}(t), & P_{bat}(t) > 0, \\ s_{chg}(t), & P_{bat}(t) < 0. \end{cases}$$

This equivalence factor is used to convert battery power into an equivalent amount of fuel, representing how much fuel would be needed, on average, to generate or recover that electrical energy. ECMS is executed in the following steps:

1. From the given states of the system, decide the acceptable range of control where the instantaneous constraints are satisfied;
2. Discretize the control interval into a finite number of control inputs;
3. Calculate the equivalent fuel consumption $\dot{m}_{f,eqv}(t)$ for each control input;
4. Select the control value P_{bat} that minimizes $\dot{m}_{f,eqv}(t)$.

The challenge with ECMS is that the value of the equivalence factor for charge s_{chg} and discharge s_{dis} must be selected beforehand. To guarantee that $SOC_{min} \leq SOC \leq SOC_{max}$, a multiplicative penalty function, $p(SOC)$ is often used:

$$\dot{m}_{f,eqv}(t) = \dot{m}_f + \frac{s(t)}{Q_{lhv}} P_{bat}(t) p(SOC). \tag{2.40}$$

$p(SOC)$ is the measure of deviation between the current SOC and the target SOC_{target} with the following equation:

$$p(SOC) = 1 - \left(\frac{SOC(t) - SOC_{target}}{(SOC_{max} - SOC_{min})/2} \right)^a, \tag{2.41}$$

where a is an arbitrary number. An analytical solution of the ECMS can also be calculated using the power-based PMP formulation [17]. The Hamiltonian is:

$$H = P_{fuel} + \lambda(t) \cdot P_{ech}(t). \tag{2.42}$$

Multiplying Equation (2.36) or (2.40) with Q_{lhv} gives the instantaneous cost:

$$P_{eqv}(t) = P_{fuel}(t) + s(t) \cdot P_{bat}(t) \tag{2.43}$$

There are similarities between Equation (2.42) and (2.43). If one assumes that the relation between the electric power P_{bat} in (2.42) and P_{ech} in (2.43) can be represented as a battery charge/discharge efficiency η_{batt}:

$$P_{ech}(SOC(t), P_{bat}(t)) = \begin{cases} \dfrac{P_{bat}(t)}{\eta_{bat}(SOC, P_{bat})} & P_{bat}(t) \geq 0 \\ \eta_{bat}(SOC, P_{bat}) P_{bat}(t) & P_{bat}(t) < 0, \end{cases} \tag{2.44}$$

where η_{batt} is battery efficiency. The relation between the Hamiltonian in (2.42) and the instantaneous cost (2.43) is complete with the following relation between the equivalence factors and the co-state:

$$s_{chg}(t) = \lambda(t)\, \eta_{bat} \tag{2.45}$$

$$s_{dis}(t) = \frac{\lambda(t)}{\eta_{bat}} \tag{2.46}$$

$$s_{chg}(t) = \eta_{bat}^2\, s_{dis}(t) \tag{2.47}$$

Both PMP and ECMS are optimal control methods with instantaneous minimization and guarantee optimality as long as the driving cycle is perfectly known [17]. The challenge with both PMP and ECMS is deciding a good initial value for λ_0 and $[s_{chg}, s_{dis}]$, respectively, to reach optimality and charge sustainability for any given driving conditions. If the driving cycle is not perfectly known, the online solution will not be optimal.

2.3 Health-aware ECMS

Traditional ECMS for FCHEVs considers only hydrogen consumption. With the growing concern over fuel cell and battery degradation, health-aware ECMS has been developed. The key feature of health-aware ECMS is the incorporation of degradation-related factors into the cost function or objective function.

2.3.1 Fuel cell degradation model

Fuel cell degradation involves multiple components, including the catalyst, membrane and gas diffusion layer [27]. The degradation process is strongly influenced by operating conditions. Start-stop events, large load variations and extreme power demands accelerate the aging process [28][29].

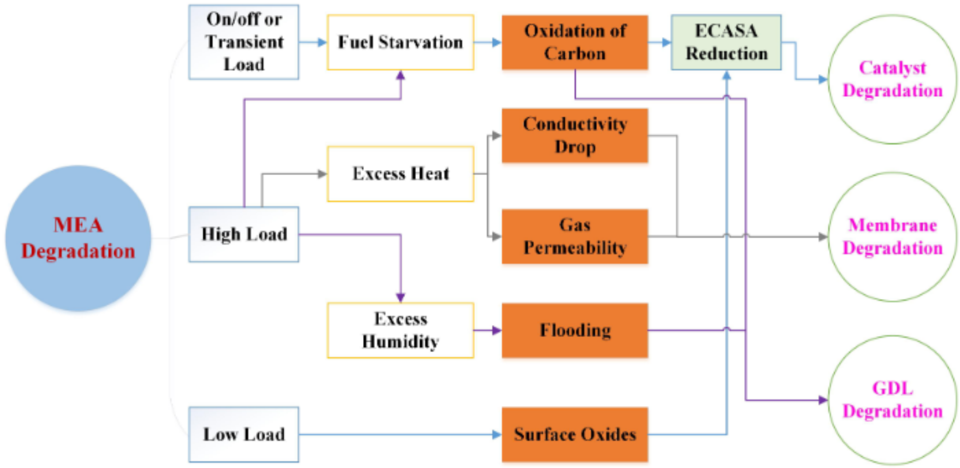

Figure 2.1: Main degradation mechanisms of fuel cells [27].

Due to the complexity of fuel cells and the difficulty of accurate modeling, most fuel cell degradation models are empirical. Among them, the most widely used approach takes output voltage decay as the aging indicator, and the end of life is defined by a voltage drop exceeding 10%. The cost or progression of fuel cell degradation is described by Equation (2.48). $C_{start-stop}$, C_{low}, C_{high} and C_{change}, derived by (2.49) - (2.52), represent the degradation costs induced by fuel cell start-stop, low working load, high working load and working load variations, respectively [30].

$$C_{fc} = C_{start\text{-}stop} + C_{low} + C_{high} + C_{change} \tag{2.48}$$

$$C_{start\text{-}stop} = \frac{\xi_{start\text{-}stop}\, N_{start\text{-}stop}\, c_{fc}}{\Delta V_{fc}} \tag{2.49}$$

$$C_{low} = \frac{\xi_{low}\, T_{low}\, c_{fc}}{\Delta V_{fc}} \tag{2.50}$$

$$C_{high} = \frac{\xi_{high}\, T_{high}\, c_{fc}}{\Delta V_{fc}} \tag{2.51}$$

$$C_{change} = \frac{\xi_{change}\, |\Delta P_{fc}|\, c_{fc}}{\Delta V_{fc}\, N_{fc}} \tag{2.52}$$

The definitions of the variables appearing in Equation (2.49)-(2.52) are given as follows. ξ_i is the degradation rate under different working conditions. c_{fc} is the price of the fuel cell system. ΔV_{fc} is the allowable voltage drop from the beginning to the end of fuel cell lifetime. $N_{start-stop}$ is the number of start and stop cycles. T_{low} and T_{high} denote the durations during which the fuel cell operates under low load or high load conditions. N_{fc} is the number of fuel cells in the stack.

Table 2.1: Fuel cell voltage degradation rate under different working conditions [31].

Working conditions	Degradation rate
Start-stop	$\xi_{start-stop} = 13.79\ \mu\text{V/cycle}$
Low load (Power below 20% of rated power)	$\xi_{low} = 8.662\ \mu\text{V/h}$
High load (Power above 80% of rated power)	$\xi_{high} = 10.00\ \mu\text{V/h}$
Load change	$\xi_{change} = 0.04185\ \mu\text{V/kW}$

2.3.2 Battery degradation model

In vehicular applications, lithium-ion battery is the most widely adopted battery technology. Lithium-ion battery degradation is primarily driven by side reactions, such as anode-electrolyte reactions and metallic lithium plating. These degradation mechanisms are affected by temperature, SOC, depth of discharge, and charge/discharge rates [27].

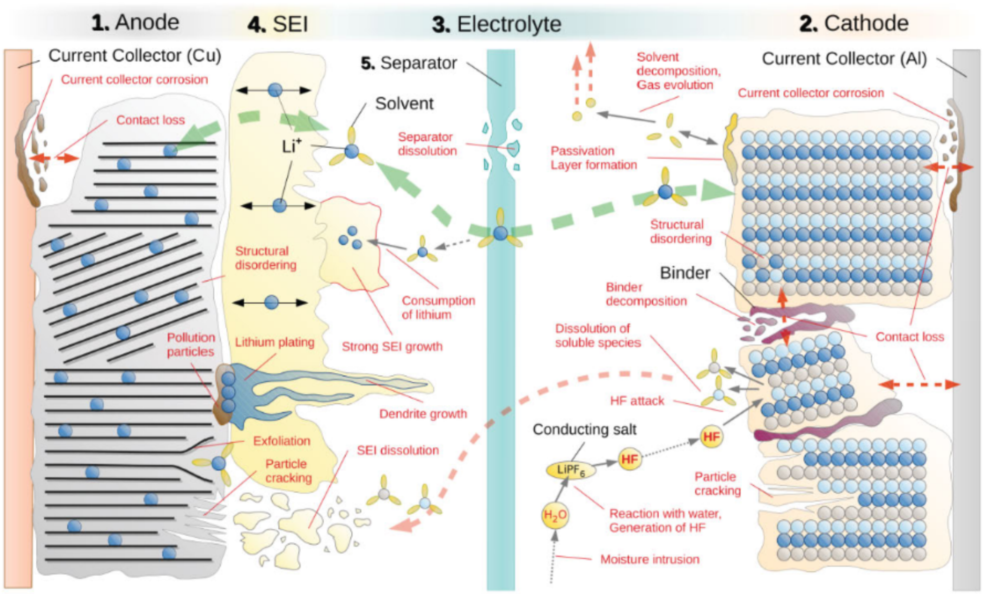

Figure 2.2: Main degradation mechanisms of lithium-ion batteries [27].

Considering applicability, complexity and accuracy, semi-empirical models are the most promising approach for describing lithium-ion battery degradation. A widely adopted model estimates capacity loss using the following equation [31]:

$$\Delta Q = b(c) \exp\left(-\frac{E_a(c)}{RT_a}\right) A(c)^z, \tag{2.53}$$

where ΔQ is denotes the battery capacity loss expressed as a percentage (%). $b(c)$ is the pre-exponential factor dependent on the C-rate c, as summarized in Table 2.2. R is the ideal gas constant. T_a is the battery temperature. $A(c)$ is the ampere-hour throughput. z is a power-law factor, which is set to 0.55. $E_a(c)$ is the activation energy and is given by

$$E_a(c) = 31700 - 370.3c. \tag{2.54}$$

In the automotive industry, a battery is typically considered to have reached its end of life when its capacity has decreased by 20%. Under this criterion, the total throughput A_{EOL} can be calculated as

$$A_{EOL} = \left[\frac{20}{b(c) \exp\left(\frac{E_a(c)}{RT_a} \right)} \right]^{\frac{1}{z}}. \tag{2.55}$$

Then the total number of equivalent full cycles throughout the battery lifetime can be determined as

$$N_{EOL} = \frac{A_{EOL}}{2\,Q_{nom}}. \tag{2.56}$$

Finally, the cost of battery degradation can be described by

$$C_{bat} = \frac{|I|\,t\,c_{bat}}{N_{EOL}\,Q_{nom}} \tag{2.57}$$

where I is the current of the battery and t is the corresponding time duration. c_{bat} is the price of the battery. Q_{nom} is the nominal capacity of the battery.

Table 2.2: Values of the pre-exponential factor $b(c)$ at different C-rates [31].

C-rate	0.5	2	6	10
b	31,630	21,681	12,934	15,512

3
Methods

To achieve the thesis objectives and address the stated research questions, a structured methodology plan was employed:

- Conduct a comprehensive review and critical assessment of current ECMS-based energy management strategies for FCHEVs. Both adaptive and health-conscious variants are investigated for identifying limitations of current energy management strategies.
- Based on insights from the literature review, alternative or improved ECMS-based solutions are proposed and developed. Appropriate degradation related cost items for FCS will be added to the cost function. The enhanced ECMS should simultaneously co-optimize hydrogen consumption as well as FCS/ESS degradation, and maintain ESS SOC within an appropriate range.
- Develop and implement efficient solution methods for the formulated ECMS problem to ensure that (quasi-)optimal results are achieved while meeting real-time computational requirements.
- Finally, the proposed ECMS is implemented on Volvo's GSP. Simulations with the original ECMS under selected representative driving cycles serve as the baseline. Performance indices such as hydrogen consumption and FCS degradation indicators are evaluated to verify the effectiveness of the proposed ECMS, and assess its advantages.

3.1 Review and assessment of current ECMS

To begin with, a literature review of existing energy management systems was conducted. The literature review was intended to explore what kinds of EMS exist, how they function, and also inspire the future work of this thesis. The literature review was extended to explore already existing health-aware EMS. Then, the current ECMS solvers in Volvo's simulation platform GSP were applied to different vehicle configurations to get an understanding of how they function and what their advantages and drawbacks are. Then multiple simulations were run to benchmark the performance of the existing solvers in GSP and then later compare them with the proposed solvers from this thesis.

The existing solvers inside GSP that are mainly studied in this thesis is called Solver 1 and Solver 3. Solver 1 is a heuristic method that performs a discretized search over feasible battery powers, evaluates the ECMS instantaneous cost, and selects the minimum-cost split. Solver 3 is an analytical ECMS solution derived from PMP. By approximating the electricity power with a second-order Taylor expansion around the previous battery power, the instantaneous minimization yields a closed-form expression for P_{bat}, which is limited by the minimum and maximum battery power.

3.2 Global Simulation Platform of Volvo

Global Simulation Platform (GSP) is an in-house developed simulation platform of Volvo Group. It is a large Simulink model of different vehicles, including BEVs, FCEVs, etc.

GSP has different model configurations suitable for different development phases. Model-in-the-Loop (MIL) is used for concept validation, Software-in-the-Loop (SIL) for software verification, and Hardware-in-the-Loop (HIL) for real-time hardware testing. As the health-aware energy management strategy is still in the development phase, this study is conducted using the MIL model.

In a specific vehicle configuration, the parameters of major components, including the battery, fuel cell system, motor, drive shaft, are predefined. Together with various controllers, driver models and driving cycles that define speed and road elevation profiles, the Simulink model enables system level simulation and performance evaluation under various operating conditions.

The ECMS module in GSP is one of the key controllers for FCEVs MIL model. It takes the total power demand together with signals from the battery and fuel cell system as inputs, and determines the optimal power split between the battery and fuel cell system as its output.

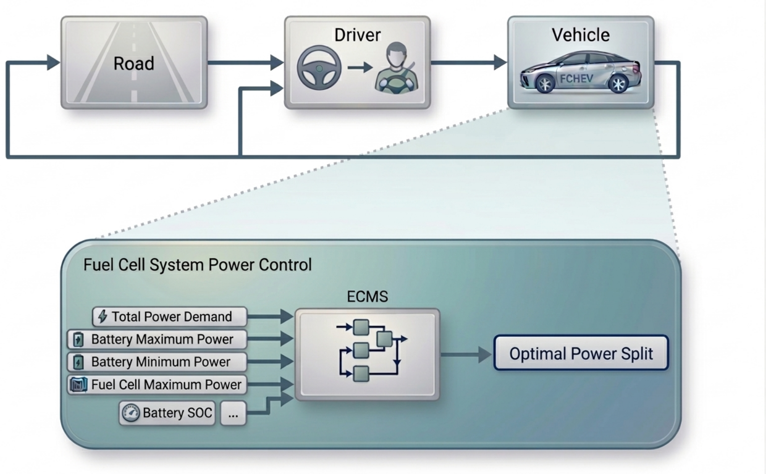

Figure 3.1: Overall architecture of Volvo GSP and the ECMS.

The proposed control algorithm is integrated into the ECMS module, and the testing and verification of the algorithm are performed on the GSP.

Although GSP is a detailed and comprehensive simulation models, it still involves certain simplifications when modeling physical systems. As a result, the outcomes of a simulation can't perfectly reflect real-world behaviors. However, such studies are still valuable for evaluating and developing control strategies before implementation on real vehicles.

3.3 Health-aware ECMS

3.3.1 Incorporating degradation effects into cost function

As mentioned before, the old ECMS module used in GSP mainly targets fuel economy by trading off hydrogen power against electricity power via an equivalence factor. At each time step, the control algorithm solve the optimization problem and find the optimal power split between battery and fuel cell, which is corresponding to the lowest cost. The cost function used is based on the power-based PMP formulation in Equation (2.43), i. e.

$$L = P_{H_2} + sP_b, \tag{3.1}$$

with P_{H_2} being hydrogen power, s the equivalence factor and P_b the battery power. The new solver introduced in this thesis is an extension of the already existing efficiency-oriented solver. To incoperate degradation-related factors into the cost function, Equation (2.48) can be used for the fuel cell degradation cost and (2.57) for the battery degradation cost. The fuel cell degradation cost is:

$$\begin{aligned} C_{fc} &= C_{start-stop} + C_{low} + C_{high} + C_{change} \\ &= \frac{\xi_{start-stop}\, N_{start-stop}\, c_{fc}}{\Delta V_{fc}} + \frac{\xi_{low}\, T_{low}\, c_{fc}}{\Delta V_{fc}} + \\ &+ \frac{\xi_{high}\, T_{high}\, c_{fc}}{\Delta V_{fc}} + \frac{\xi_{change}\, |\Delta P_{fc}|\, c_{fc}}{\Delta V_{fc}\, N_{fc}} \end{aligned} \tag{3.2}$$

In GSP, the fuel cell will remain either idle or operating after start-up, so we neglect the cost of start-stop in this research. The cost of fuel cell degradation becomes:

$$\begin{aligned} C_{fc} &= C_{low} + C_{high} + C_{change} \\ &= \frac{\xi_{low}\, T_{low}\, c_{fc}}{\Delta V_{fc}} + \frac{\xi_{high}\, T_{high}\, c_{fc}}{\Delta V_{fc}} + \frac{\xi_{change}\, |\Delta P_{fc}|\, c_{fc}}{\Delta V_{fc}\, N_{fc}} \end{aligned} \tag{3.3}$$

Based on the parameters available from the Simulink model, and to simplify the optimization problem, N_{EOL} is assumed to remain constant. The final battery degradation model is then formulated as follows:

$$C_{bat} = \frac{|I|\, t\, c_{bat}}{2\, N_{EOL}\, Q_{nom}} \tag{3.4}$$

Based on the circuit diagram in Figure 3.2 and Kirchhoff's Voltage Law, the battery current I can be calculated as follows:

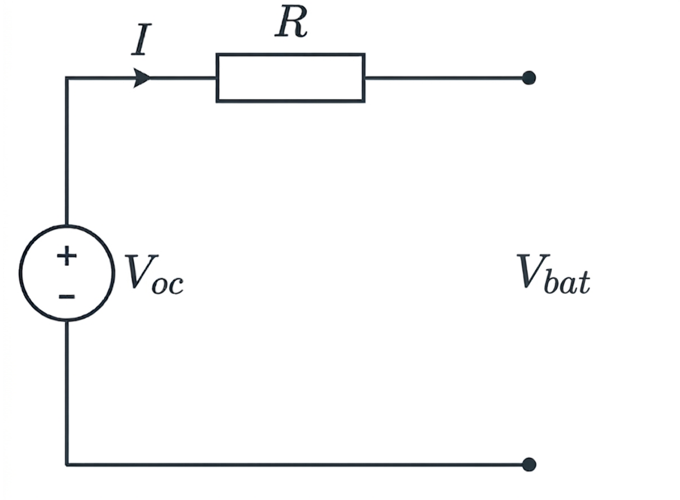

Figure 3.2: Equivalent circuit model of the battery.

$$I = \frac{V_{oc}^2 - V_{oc}\sqrt{V_{oc}^2 - 4RP_{bat}}}{2RV_{oc}} = \frac{V_{oc} - \sqrt{V_{oc}^2 - 4RP_{bat}}}{2R} \tag{3.5}$$

with P_{bat} being the battery output power, V_{oc} the open circuit voltage and R the internal resistance.

Then C_{bat} can be written as:

$$C_{bat} = \frac{|I|\, t\, c_{bat}}{2\, N_{EOL}\, Q_{nom}} = sign(P_{bat})\frac{(V_{oc} - \sqrt{V_{oc}^2 - 4RP_{bat}})\, t\, c_{bat}}{4\, R\, N_{EOL}\, Q_{nom}} \tag{3.6}$$

Since both the fuel cell and battery degradation costs are in the unit of USD, a factor of c_{H_2} has to multiplied with the already existing cost function to ensure that the unit of the cost function is consistent. The new health aware model is then:

$$L = c_{H_2}(P_{H_2} + sP_b) + C_{fc} + C_{bat} \tag{3.7}$$

where c_{H_2} denotes the hydrogen cost, with a unit of USD per Watt.

3.3.2 Analytical solution of the optimization problem

The original cost function (3.1) is a quadratic function from a Taylor expansion. A key advantage of this formulation is that it has a single extremum, which corresponds to the global optimum. The optimal solution can be obtained analytically by setting the first derivative to zero and solving the resulting equation.

The new cost function (3.7) is no longer quadratic due to the incorporation of the battery degradation cost C_{bat}. To make the new cost function quadratic and solvable by setting the partial derivative of L to zero, the battery degradation cost C_{bat} can become quadratic by making a second order Taylor expansion around $P_{bat,0}$:

$$
\begin{aligned}
C_{bat}(P_{bat}) \approx & \frac{\left|\frac{V_{oc}-\sqrt{V_{oc}^2-4RP_{bat,0}}}{2R}\right| t\, c_{bat}}{2\, N_{EOL}\, Q_{nom}} + \\
& + \frac{t\, c_{bat}}{2\, N_{EOL}\, Q_{nom}} \operatorname{sgn}(P_{bat,0}) \frac{1}{\sqrt{V_{oc}^2-4RP_{bat,0}}}(P_{bat}-P_{bat,0}) + \\
& + \frac{t\, c_{bat}}{N_{EOL}\, Q_{nom}} \operatorname{sgn}(P_{bat,0}) \frac{R}{(V_{oc}^2-4RP_{bat,0})^{3/2}}(P_{bat}-P_{bat,0})^2
\end{aligned} \tag{3.8}
$$

When the battery is being discharged, the signum function is equal to 1:

$$
\begin{aligned}
C_{bat}(P_{bat}) \approx & \frac{\left|\frac{V_{oc}-\sqrt{V_{oc}^2-4RP_{bat,0}}}{2R}\right| t\, c_{bat}}{2\, N_{EOL}\, Q_{nom}} + \\
& + \frac{t\, c_{bat}}{2\, N_{EOL}\, Q_{nom}} \frac{1}{\sqrt{V_{oc}^2-4RP_{bat,0}}}(P_{bat}-P_{bat,0}) + \\
& + \frac{t\, c_{bat}}{N_{EOL}\, Q_{nom}} \frac{R}{(V_{oc}^2-4RP_{bat,0})^{3/2}}(P_{bat}-P_{bat,0})^2
\end{aligned} \tag{3.9}
$$

When the battery is being charged, the signum function is equal to -1:

$$
\begin{aligned}
C_{bat}(P_{bat}) \approx & \frac{\left|\frac{V_{oc}-\sqrt{V_{oc}^2-4RP_{bat,0}}}{2R}\right| t\, c_{bat}}{2\, N_{EOL}\, Q_{nom}} - \\
& - \frac{t\, c_{bat}}{2\, N_{EOL}\, Q_{nom}} \frac{1}{\sqrt{V_{oc}^2-4RP_{bat,0}}}(P_{bat}-P_{bat,0}) - \\
& - \frac{t\, c_{bat}}{N_{EOL}\, Q_{nom}} \frac{R}{(V_{oc}^2-4RP_{bat,0})^{3/2}}(P_{bat}-P_{bat,0})^2
\end{aligned} \tag{3.10}
$$

Although the new cost function is now quadratic, because of the absolute values in C_{change} and C_{bat}, it is not differentiable. To deal with this issue, the cost function can be further split into a piecewise function.

In C_{change}, the change of the fuel cell power ΔP_{fc} may be either positive or negative, and similarly, the battery current I can take both positive and negative values. Considering different combination of these conditions, the cost function can be formulated as a four-segment piecewise function as follows:

$$L_1 = ... + \frac{\xi_{change}\overbrace{(P_{dem} - P_{bat} - P_{fc,old})}^{\Delta P_{fc}>0}c_{fc}}{\Delta V_{fc} N_{fc}} + \frac{\left(\overbrace{\frac{V_{oc} - \sqrt{V_{oc}^2 - 4RP_{bat,0}}}{2R}}^{I\geq 0}\right) t\, c_{bat}}{2\, N_{EOL}\, Q_{nom}} + ... \tag{3.11}$$

$$L_2 = ... + \frac{\xi_{change}\overbrace{(P_{dem} - P_{bat} - P_{fc,old})}^{\Delta P_{fc}>0}c_{fc}}{\Delta V_{fc} N_{fc}} + \frac{(-1)\left(\overbrace{\frac{V_{oc} - \sqrt{V_{oc}^2 - 4RP_{bat,0}}}{2R}}^{I<0}\right) t\, c_{bat}}{2\, N_{EOL}\, Q} + ... \tag{3.12}$$

$$L_3 = ... + \frac{\xi_{change}(-1)\overbrace{(P_{dem} - P_{bat} - P_{fc,old})}^{\Delta P_{fc}\leq 0}c_{fc}}{\Delta V_{fc} N_{fc}} + \frac{\left(\overbrace{\frac{V_{oc} - \sqrt{V_{oc}^2 - 4RP_{bat,0}}}{2R}}^{I\geq 0}\right) t\, c_{bat}}{2\, N_{EOL}\, Q_{nom}} + ... \tag{3.13}$$

$$L_4 = ... + \frac{\xi_{change}(-1)\overbrace{(P_{dem} - P_{bat} - P_{fc,old})}^{\Delta P_{fc}\leq 0}c_{fc}}{\Delta V_{fc} N_{fc}} + \frac{(-1)\left(\overbrace{\frac{V_{oc} - \sqrt{V_{oc}^2 - 4RP_{bat,0}}}{2R}}^{I<0}\right) t\, c_{bat}}{2\, N_{EOL}\, Q_{nom}} + ... \tag{3.14}$$

Here, the ellipses indicate omitted identical items, specifically the hydrogen cost term at the beginning and the last two terms in Equation (3.9) and (3.10) in the end, in order to highlight the differences between individual segments.

According to Equation (3.3), C_{low} and C_{high} are dependent on the load time durations T_{low} and T_{high}. In GSP, the fuel cell power remains constant within each simulation time step. Therefore, T_{low} and T_{high} are equal to the simulation time step, the only factor determining the degradation cost is the load region in which the system operates.

Then for each segment of the piecewise function defined before, the final cost function can be expressed as follows:

$$L_{1,final} = \begin{cases} L_1 + C_{low}, & P_{fc} < P_{fc,low} \\ L_1, & P_{fc,low} \leq P_{fc} < P_{fc,high} \\ L_1 + C_{high}, & P_{fc} \geq P_{fc,high} \end{cases} \tag{3.15}$$

In summary, each segment is associated with three possible operating regions, resulting in a total of twelve cases, which are listed in Table 3.1.

Table 3.1: Twelve-segment piecewise cost function definition.

	I	ΔP_{fc}	Load region	Cost funtion
Case 1	> 0	>0	High load	$L_1 + C_{high}$
Case 2	> 0	>0	Normal load	L_1
Case 3	> 0	>0	Low load	$L_1 + C_{low}$
Case 4	<0	>0	High load	$L_2 + C_{high}$
Case 5	<0	>0	Normal load	L_2
Case 6	<0	>0	Low load	$L_2 + C_{low}$
Case 7	> 0	<0	High load	$L_3 + C_{high}$
Case 8	> 0	<0	Normal load	L_3
Case 9	> 0	<0	Low load	$L_3 + C_{low}$
Case 10	<0	<0	High load	$L_4 + C_{high}$
Case 11	<0	<0	Normal load	L_4
Case 12	<0	<0	Low load	$L_4 + C_{low}$

Finally, the cost function for each case is differentiable and the derivative of the cost function with respect to P_{bat} can be calculated. With the help of the MATLAB Symbolic Toolbox, the solution satisfying the condition that the derivative of the cost function equals zero can be obtained. For the piecewise quadratic function in each case, if the stationary point does not lie within the feasible region, the optimal solution lies on the boundary defined by the active constraints. Based on this, the optimal solution for each case can be derived.

There are twelve local optimal solutions and each one of them is evaluated using the cost function. The solution that yields the lowest cost is selected as the global optimal solution.

The steps for deriving the analytical solution are summarized in Figure 3.3

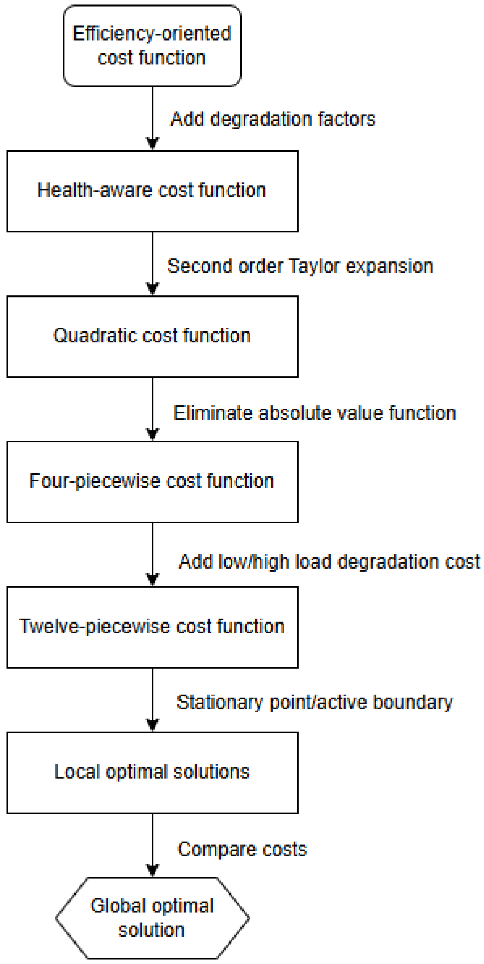

Figure 3.3: Flowchart of the procedure for obtaining the analytical solution.

4
Results

In this chapter, the simulation results that have been used to evaluate the performance of energy management strategies are presented. The results are analyzed from multiple different driving cycles, representing different driving conditions, to ensure a thorough assessment.

To begin with, the evaluation metrics used to quantify energy efficiency and component degradation are presented, followed by an explanation of the different driving cycles used in the simulations. To conclude this chapter, the results of conventional solvers are presented and compared to the proposed health-aware one, to spot differences in performance and system behavior.

4.1 Evaluation Metrics

After implementing the proposed health-aware solver in GSP, a set of evaluation metrics is required to quantitatively compare the results of the conventional and the proposed solvers. Indicators such as degradation level, system efficiency, and drivability should be comprehensively considered.

Rainflow count: The rainflow function in MATLAB enables fatigue analysis by quantifying load change cycles with respect to their amplitudes. Since fuel cell degradation is strongly associated with load transients and operation under high and low load conditions, the rainflow method is well suited for evaluating fuel cell degradation over a specific driving cycle. With the help of the MATLAB rainflow function, the rainflow count of the fuel cell can be calculated. Moreover, the load change range can be flexibly selected to focus on specific regions of interest as needed.

ESS throughput: As discussed in Section 2.3.2, battery capacity degradation is largely affected by the ampere-hour throughput. Therefore, the ESS throughput over a specific driving cycle can serve as an effective indicator of battery health.

SOC deviation: The FCHEVs investigated in this study are not plug-in hybrids and therefore must operate under a charge-sustaining strategy. In other words the end SOC should be close the initial SOC. The fuel cell serves as the primary energy source, while the battery acts as an energy buffer, providing supplementary power and enabling regenerative energy recovery. The SOC deviation is therefore used as an indicator to evaluate the energy balance of the system.

Compensated fuel consumption: For a given driving cycle, hydrogen consumption can be directly compared to evaluate system efficiency when there is no SOC deviation. However, when there is a SOC deviation, a compensated hydrogen consumption must be considered. Based on fuel cell efficiency, the energy used by the battery can be converted into an equivalent hydrogen consumption. By adding this term to the actual hydrogen consumption, the compensated fuel consumption can be obtained.

Drivability: In this study, drivability refers to the ability of the vehicle to follow a predefined speed profile. For a constant reference speed, it can be quantitatively evaluated by comparing the average speed with the reference speed. When the reference speed is time-varying, a qualitative assessment of the speed profile is adopted to simplify the evaluation.

4.2 Test driving cycles settings

To assess the adaptability of the proposed health-aware controller under different road profiles, various driving cycles are established for simulation.

The driving cycles used in this study are illustrated in Figure 4.1. Three representative cycles with different characteristics are considered. The normal driving cycle is approximately 90 km in length, with road inclinations within $\pm 5\%$. The hilly driving cycle is about 120 km, with inclinations within $\pm 10\%$, and exhibits more rapid slope variations. The long driving cycle covers approximately 650 km and includes a relatively long downhill segment towards the end.

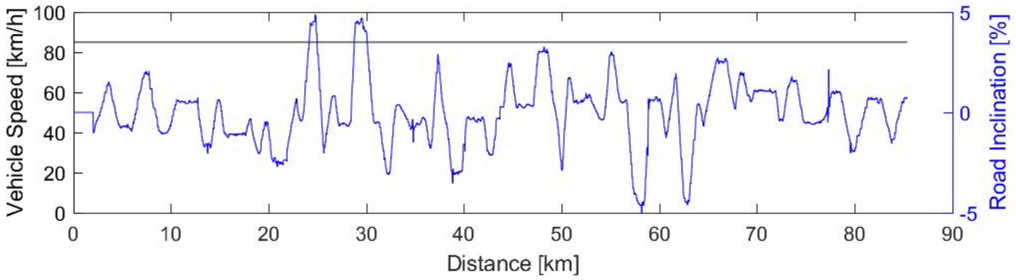

(a) Normal driving cycle (BLB)

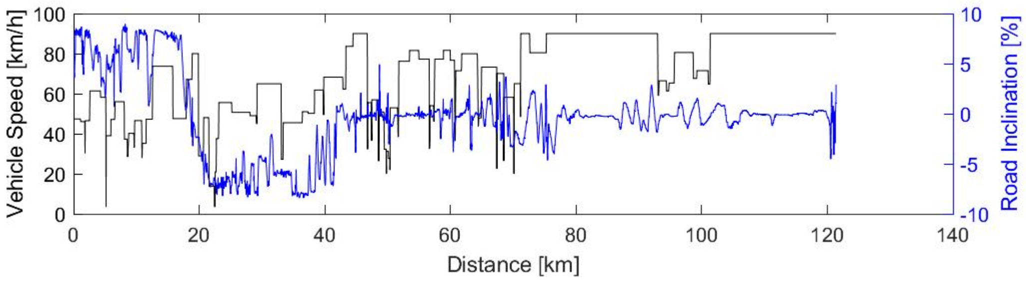

(b) Hilly driving cycle (sx314b)

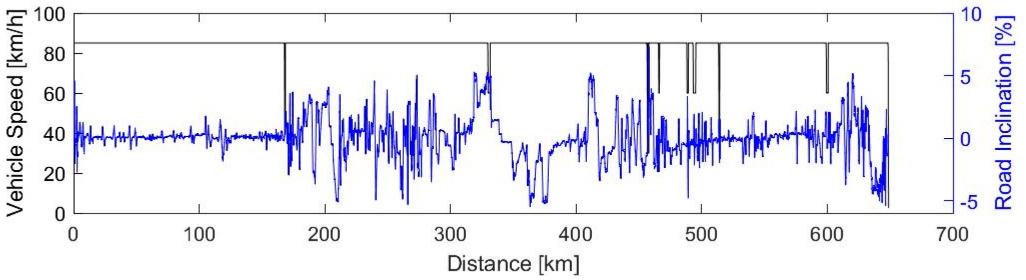

(c) Long driving cycle (sx1148b)

Figure 4.1: Representative driving cycles used in this study.

4.3 Simulation results of old solvers

The simulation result of a normal driving cycle for the heuristic method of Solver 1 can be seen in Figure 4.2. For the same driving cycle the simulation result of the analytical solution, Solver 3 can be seen in Figure 4.3. In both Figure 4.2 and 4.3 the fuel cell power output is not smooth and the battery power have spikes in the output and is not smooth either. This results in faster aging of the battery and fuel cell.

In some cases, the battery output power can be observed to exceed its prescribed boundary. This is due to the post-processing module in GSP after the ECMS controller, which modifies the final power command before it is sent to the battery plant. To satisfy the overall power request, the battery power may therefore temporarily exceed its boundary.
Small violations of the battery power constraints can be observed in some simulations. These violations arise because the battery power limits are implemented as

soft constraints within the optimization framework. Soft constraints allow limited violations when necessary to maintain feasibility and avoid excessively conservative control actions. Although the constraints are temporarily exceeded, the magnitude and duration of the violations are small and do not significantly affect vehicle operation. However, such violations should be considered when evaluating the practical implementation of the controller.

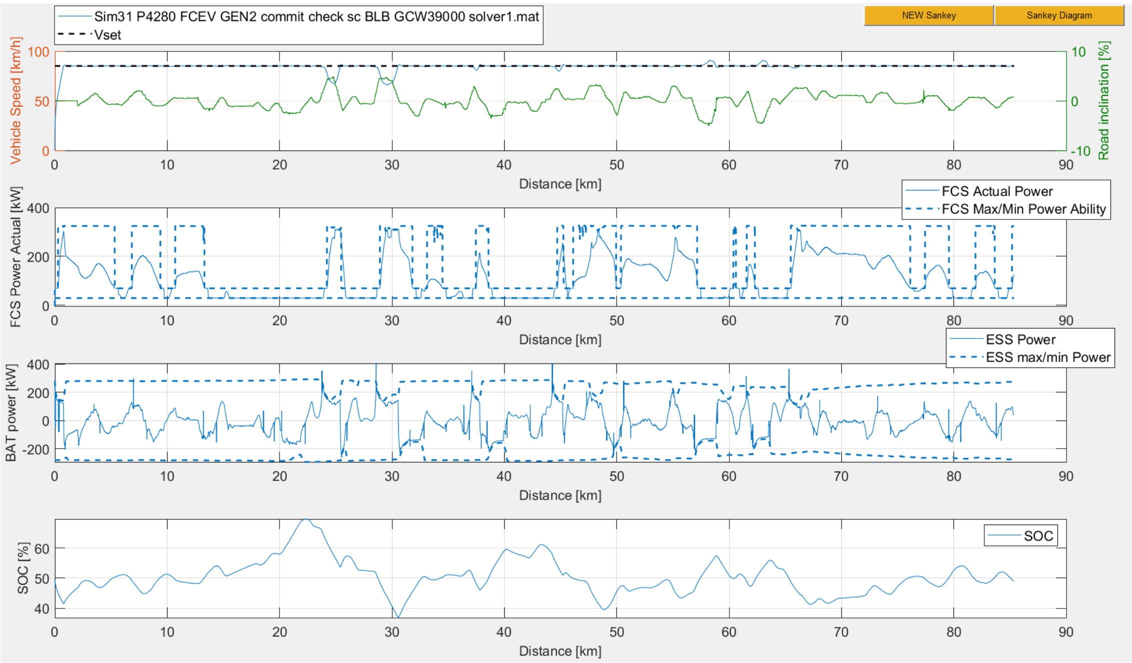

Figure 4.2: Simulation results for Solver 1 in driving cycle BLB.

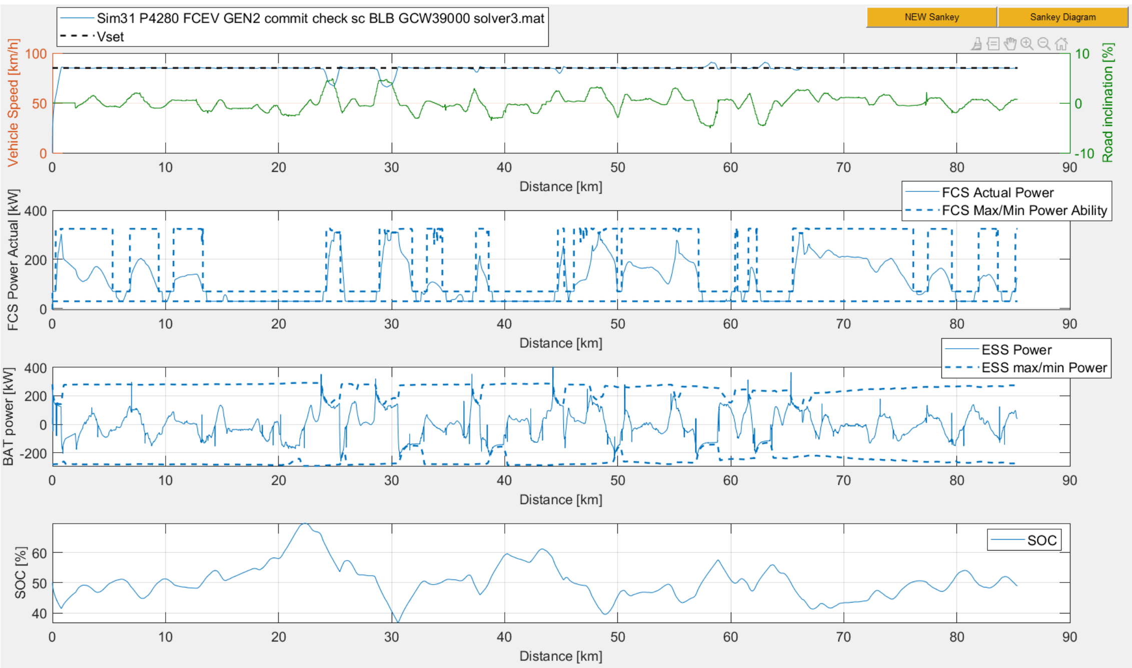

Figure 4.3: Simulation results for Solver 3 in driving cycle BLB.

The specific numbers of how Solver 1 and 3 compare in a normal driving cycle can be seen in Table 4.1. Solver 3 has 3.6 % lower Rainflow count compared to Solver 1, Solver 3 has 0.05 % lower ESS throughput compared to solver 1. Solver 1 and 3 have the same fuel consumption, and the same SOC at the end of the driving cycle, though Solver 3 has 0.07 % higher average speed.

Table 4.1: Performance metrics Solver 1 and 3 in driving cycle BLB.

	Solver 1	Solver 3
Rainflow count (1/h)	27.01	26.03
ESS throughput (kW)	76.27	76.23
Fuel consumption (kg/100km)	7.97	7.97
End SOC (%)	49	49
Average speed (km/h)	83.86	83.92

In a driving cycle with many hills, the simulation results of Solver 1 can be seen in Figure 4.4 and for Solver 3 the simulation results can be seen in Figure 4.5. In both the plot of Solver 1 and 3 the fuel cell power output is not smooth and there are spikes. In the battery power output there are oscillations. These are all factors contributing to faster aging of the fuel cell and battery. Again, small violations of the battery power constraints can be observed since the battery power limits are implemented as soft constraints.

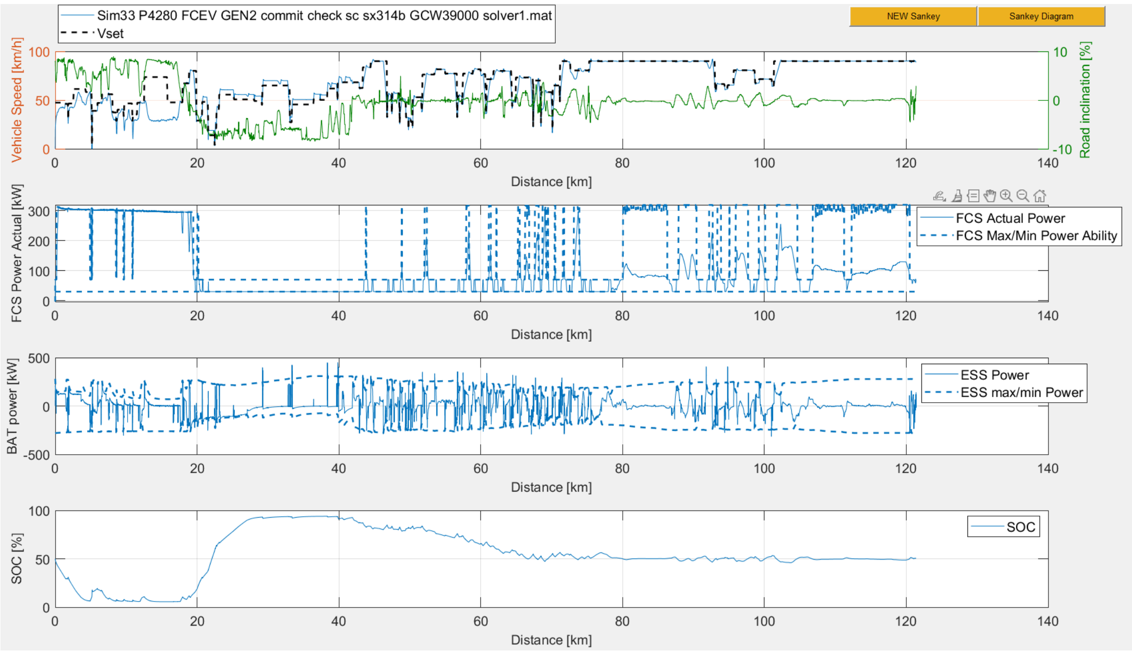

Figure 4.4: Simulations results for Solver 1 in driving cycle sx314b.

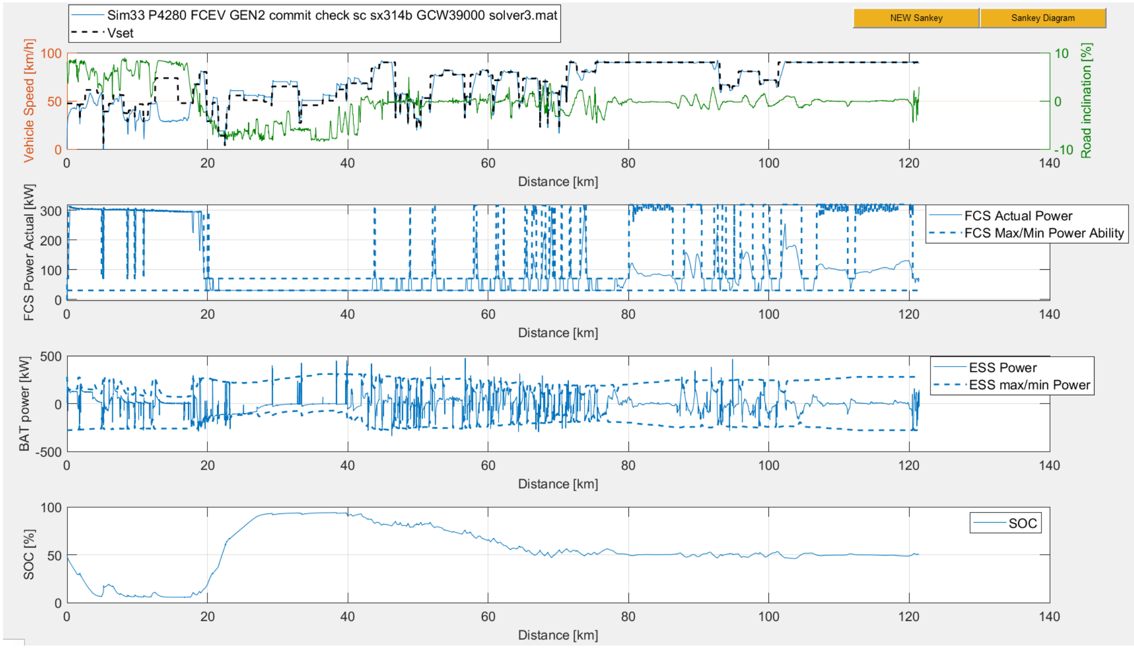

Figure 4.5: Simulation results for Solver 3 in driving cycle sx314b.

A comparison of the simulation result of Solver 1 and 3 can be seen in Table 4.2. Solver 3 has 3.2 % lower Rainflow count compared to Solver 1, and Solver 1 has 0.03 % lower ESS throughput compared to Solver 3. Solver 1 and 3 have the same fuel consumption, the same SOC at the end of the driving cycle and the same average speed.

Table 4.2: Performance metrics Solver 1 and 3 in driving cycle sx314b.

	Solver 1	Solver 3
Rainflow count (1/h)	30.32	29.35
ESS throughput (kW)	66.0	66.02
Fuel consumption (kg/100km)	13.06	13.06
End SOC (%)	50	50
Average speed (km/h)	58.88	58.88

For a long driving cycle, the simulation results of Solver 1 can be seen in Figure 4.6 and for Solver 3 the simulation results can be seen in Figure 4.7. In both the plots of Solver 1 and 3 the fuel cell power output is not smooth and there are spikes. In the battery power output there are oscillations. These are all factors contributing to faster aging of the fuel cell and battery. This behavior is consistent across all three driving cycles. The lack of smoothness is because there is no direct penalty for power variation, which causes the controller to react aggressively to instantaneous load changes.

In both Figure 4.6 and 4.7 there are small violations of the battery power constraints since again the battery power limits are implemented as soft constraints.

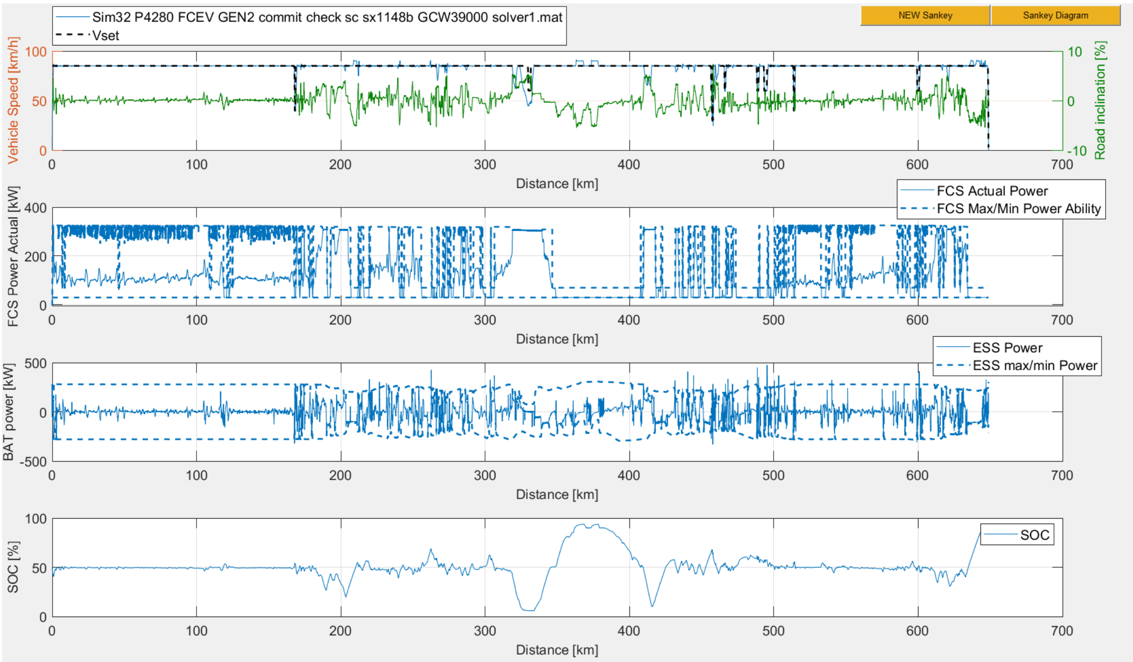

Figure 4.6: Simulations results for Solver 1 in driving cycle sx1148b.

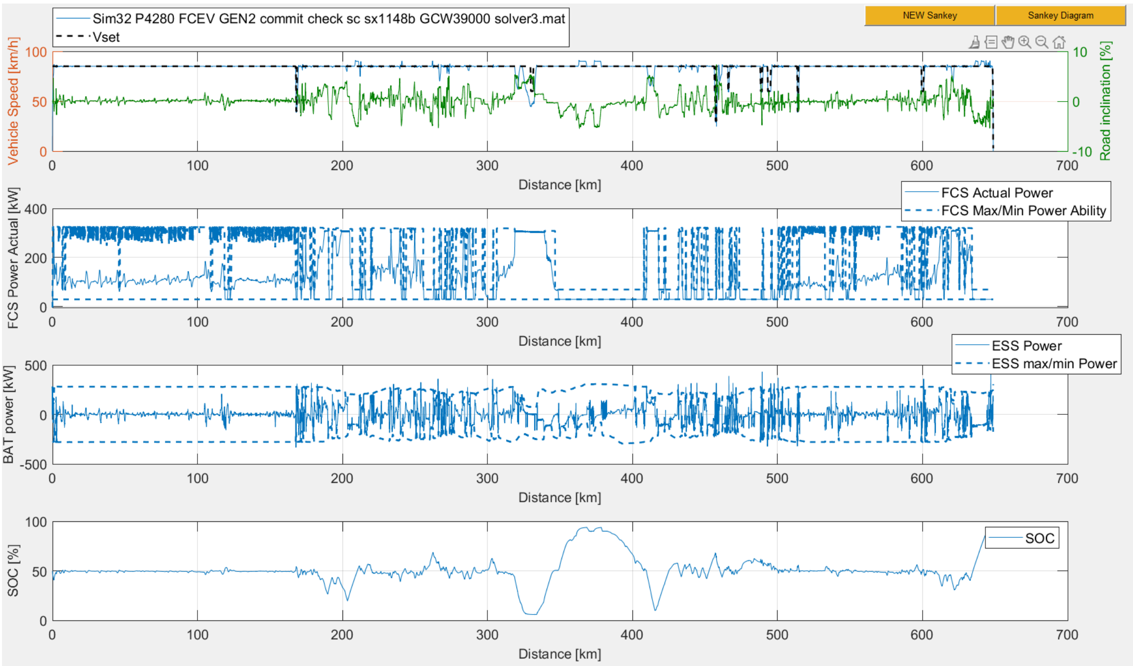

Figure 4.7: Simulation results for Solver 3 in driving cycle sx1148b.

A comparison of the simulation results of Solver 1 and 3 can be seen in Table 4.3. Solver 3 has 1.7 % lower Rainflow count, and 0.08 % lower ESS throughput compared to Solver 1. Solver 1 and 3 have the same fuel consumption, SOC at the end of the driving cycle, and average speed.

Table 4.3: Performance metrics Solver 1 and 3 in driving cycle sx1148b.

	Solver 1	Solver 3
Rainflow count (1/h)	26.83	26.33
ESS throughput (kW)	51.30	51.26
Fuel consumption (kg/100km)	8.56	8.56
End SOC (%)	90	90
Average speed (km/h)	81.32	81.32

Despite the different approaches in Solver 1 and 3, the performance is similar across and the three driving cycles. The main reason for the similarities in performance is that both solvers use the same ECMS formulation, and they both minimize the same cost function. Solver 1 performs a discretized search over feasible battery power values, while Solver 3 derives an analytical solution using a quadratic approximation. However, since both solvers have the same objective, their control actions and performance metrics are nearly identical. This indicates that the solution method of the power split problem has limited impact on performance.

In all three driving cycles, both Solver 1 and Solver 3 exhibit oscillatory and non-smooth behavior in the battery and fuel cell power outputs. This is reflected in the relatively high rainflow counts and the visible power fluctuations in Figures 4.2, 4.3, 4.4, 4.5, 4.6 and 4.7. The primary reason for this behavior is that both solvers are designed to minimize an instantaneous cost function that considers only fuel consumption and equivalent electrical energy, without accounting for component degradation or power smoothness. As a result, the optimization favors rapid changes in power split whenever a lower instantaneous cost can be achieved, leading to frequent switching and oscillations.

Although this strategy can achieve near-optimal energy efficiency in the short term, it does so at the expense of increased stress on the fuel cell and battery, which may accelerate degradation. From a lifecycle perspective, neglecting degradation effects can lead to higher overall system costs, as reduced component lifetime necessitates more frequent replacement. This limitation motivates the development of health-aware energy management strategies that explicitly incorporate degradation into the optimization problem.

4.4 Simulation results of new solver

For comparison of the performance of the new health-aware solver with old solvers, Solver 1 will be used as benchmark since the performance of Solver 1 and 3 is similar. The simulation result of a normal driving cycle can be seen in Figure 4.8. Compared with Solver 1, the newly developed Solver 0 yields a smoother fuel cell power output, which implies a reduction in fuel cell degradation. Once again, some small violations of the battery power constraints can be observed since the battery power limits are implemented as soft constraints here as well.

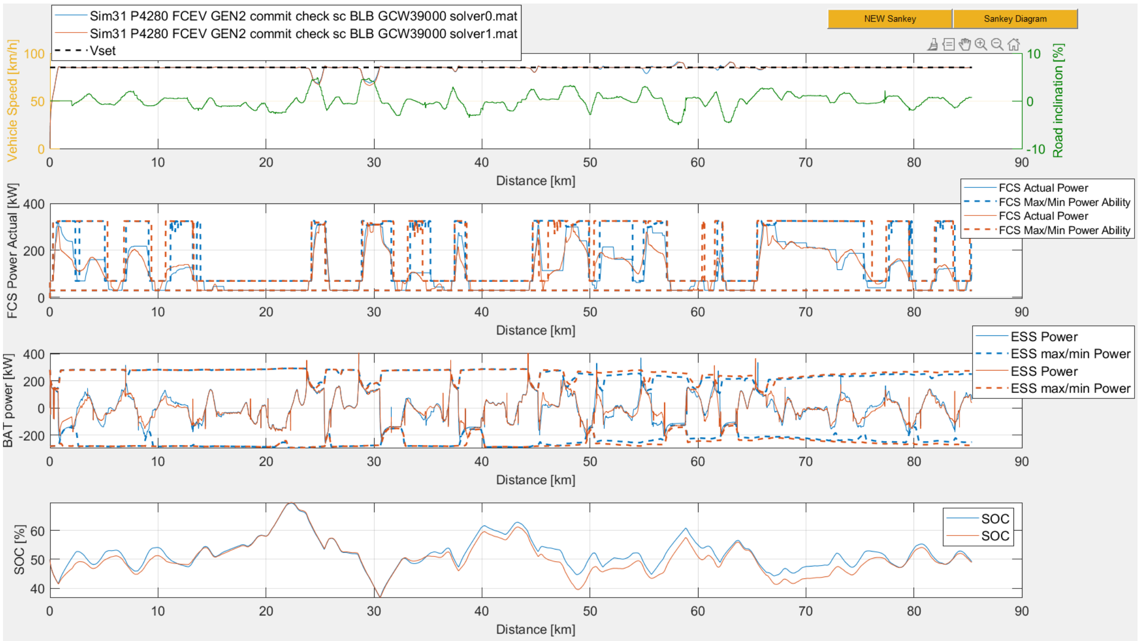

Figure 4.8: Simulation results for Solver 0 and 1 in driving cycle BLB.

A comparison of the simulation result of Solver 1 and Solver 0 can be seen in Table 4.4. Compared with Solver 1, Solver 0 reduces the rainflow count by 25.4%, while increasing the ESS throughput by 10.0%. This trade-off is expected, since the combined output power of the fuel cell and battery should satisfy the total system power demand. Consequently, a smoother fuel cell power output tends to shift more dynamic load to the battery, which may lead to increased battery degradation, highlighting the need for balanced degradation modeling of both components.

The fuel consumption of Solver 0 increases by 6.8% compared with Solver 1. This increase is expected, as the control objective transitions from minimizing fuel consumption alone to considering both efficiency and the components health.

The end SOC is identical for both solvers. There is no difference in charge sustaining performance.

For this driving cycle, the reference speed is set to 85 km/h. Solver 0 exhibits a slightly higher average speed compared to Solver 1, indicating better drivability.

Table 4.4: Performance metrics for Solver 0 and 1 in driving cycle BLB.

	Solver 0	Solver 1
Rainflow count (1/h)	20.15	27.01
ESS throughput (kW)	83.90	76.27
Fuel consumption (kg/100km)	8.51	7.97
End SOC (%)	49	49
Average speed (km/h)	83.90	83.86

The simulation result of a hilly driving cycle can be seen in Figure 4.9. Similar to the normal driving cycle, the newly developed Solver 0 yields a smoother fuel cell power output. At the same time, the battery output power of both solvers exhibits similar behavior.

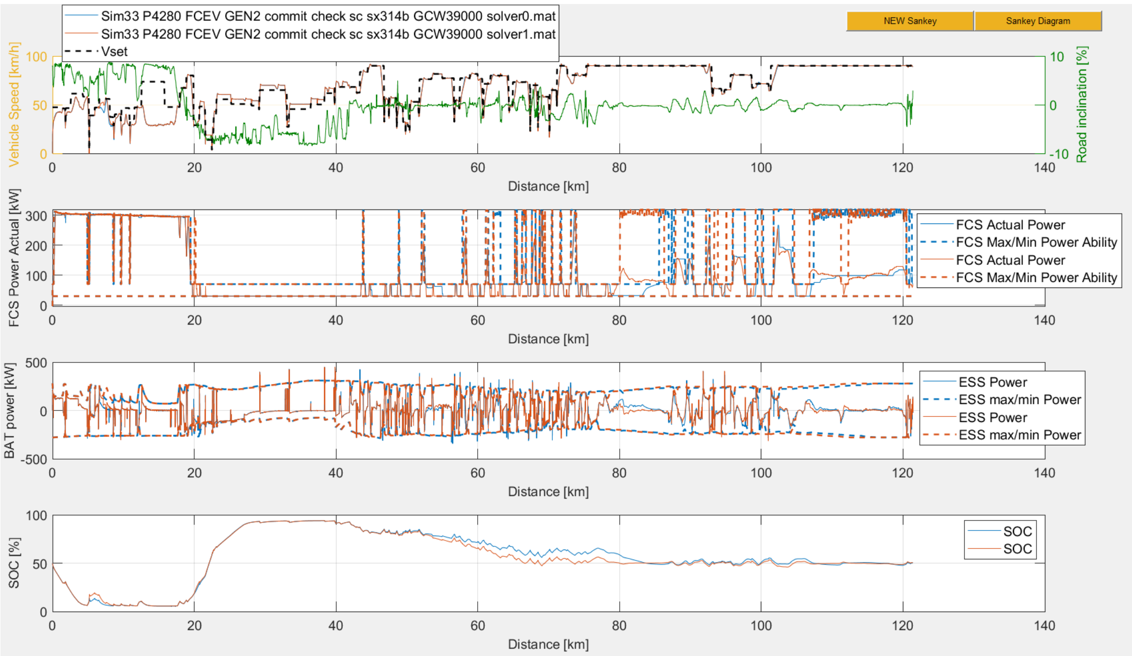

Figure 4.9: Simulation results for Solver 0 and 1 in driving cycle sx314b.

A comparison of the simulation result of Solver 1 and Solver 0 can be seen in Table 4.5. Compared with Solver 1, Solver 0 reduces the rainflow count by 29.7%, while slightly increasing the ESS throughput by 1.8%. Battery degradation increase is less significant compared to the normal driving cycle. This can be attributed to the presence of frequent downhill segments in the hilly driving cycle, during which the fuel cell operates within a relatively low and narrow power. As a result, adjustments to the fuel cell output power have a limited influence on battery output power.

The fuel consumption of Solver 1 exhibits no significant difference compared with Solver 0.

The end SOC is identical for both solvers. There is no difference in charge sustaining performance.

For this driving cycle, the reference speed is not set to a constant value. From a qualitative perspective, Solver 0 shows slightly worse drivability than Solver 1, as a small speed drop is observed within the first 10 km.

Table 4.5: Performance metrics for Solver 0 and 1 in driving cycle sx314b.

	Solver 0	Solver 1
Rainflow count (1/h)	21.30	30.32
ESS throughput (kW)	67.20	66.0
Fuel consumption (kg/100km)	13.0	13.06
End SOC (%)	50	50
Average speed (km/h)	58.75	58.88

The simulation result of a long driving cycle can be seen in Figure 4.10. Similar to the normal and hilly driving cycle, the newly developed Solver 0 yields a smoother fuel cell power output.

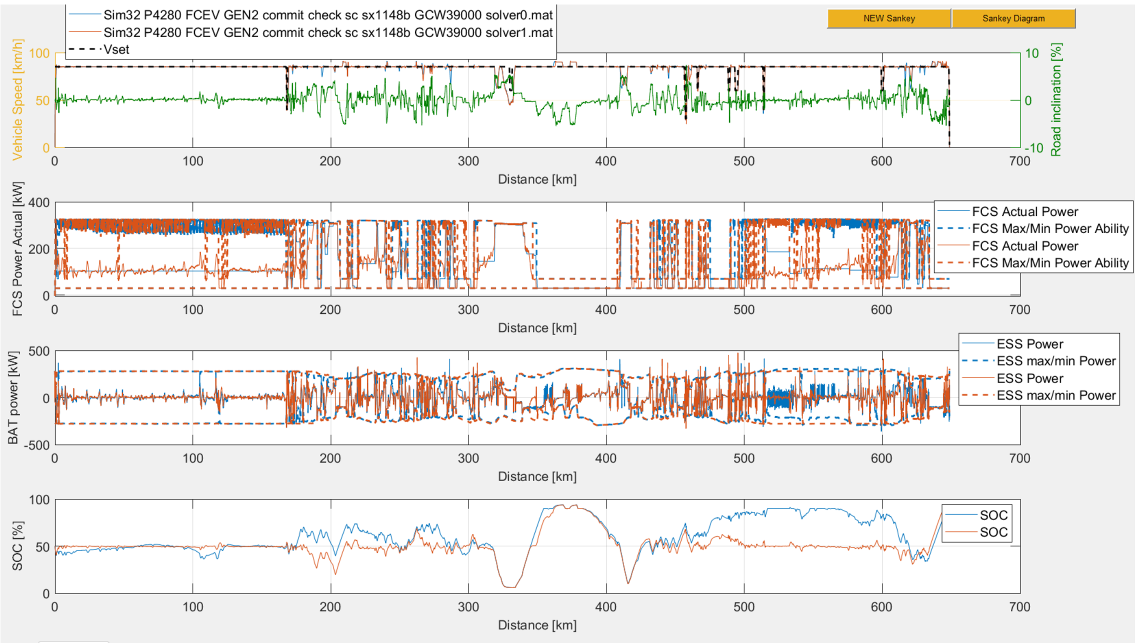

Figure 4.10: Simulation results for Solver 0 and 1 in driving cycle sx1148b.

A comparison of the simulation result of Solver 1 and Solver 0 can be seen in Table 4.6. Compared with Solver 1, Solver 0 reduces the rainflow count by 76.7%, while increasing the ESS throughput by 13.9%. The mitigation effect on fuel cell degradation is more significant than normal and hilly driving cycles, indicating that Solver 0 is particularly effective in reducing fuel cell aging during long driving cycles, where cumulative stress effects are most critical.

The fuel consumption of Solver 0 increases by 2.6% compared with Solver 1.

The end SOC is identical for both solvers, demonstrating comparable charge sustaining performance. However, the end SOC reaches 90%, which deviates from the initial value of 50%. This increase is primarily due to the downhill segment at the end of the driving cycle, during which regenerative braking contributes to additional battery charging.

For this driving cycle, the reference speed is also not set to a constant value. From a qualitatively perspective, Solver 0 shows slightly worse drivability than Solver 1, as more speed drops can be observed.

Table 4.6: Performance metrics for Solver 0 and 1 in driving cycle sx1148b.

	Solver 0	Solver 1
Rainflow count (1/h)	6.26	26.83
ESS throughput (kW)	58.45	51.30
Fuel consumption (kg/100km)	8.78	8.56
End SOC (%)	90	90
Average speed (km/h)	81.25	81.32

Overall, across all three driving cycles, the result shows that the proposed health-aware solver can consistently reduce fuel cell cycling under different operating conditions, with the result that in long and dynamic conditions the greatest improvements are experienced. This shows that incorporating degradation terms into the cost function changes the control strategy, encouraging smoother fuel cell power output with a slight expense of increased battery cycling and marginally higher fuel consumption.

5
Conclusions and Future work

In this chapter, the thesis is concluded with a summary of the main findings. These findings are discussed in relation to the scope of the research. In addition to this, limitations with the current study are identified and suggestions for future research are presented.

5.1 Conclusions

The main contributions of this thesis are as follows.

- First, the conventional ECMS cost function is reformulated to incorporate degradation effects of both the fuel cell system and the battery, enabling a health-aware energy management strategy rather than a purely efficiency-driven one.

- Second, the resulting non-linear and non-differentiable optimization problem is addressed by deriving an analytical solution through piecewise quadratic approximation, allowing real-time applicability despite the added complexity.

- Finally, the proposed method is implemented and evaluated within Volvo's GSP, enabling realistic system-level validation under representative driving conditions. The simulation results show that the proposed method can significantly mitigate fuel cell degradation, with an acceptable increase in battery degradation and fuel consumption. Meanwhile, the charge sustaining performance and drivability are largely preserved.

The results show that the proposed method considerably changes the behavior of the system compared to conventional ECMS. In particular, the fuel cell output becomes smoother, which reduces the fuel cell cycling. The rainflow count is reduced by up to 77% in long driving cycles, indicating a strong potential to reduce fuel cell degradation. At the same time, fuel consumption stays roughly the same, but in some cases there is a slight increase in fuel consumption.

This improvement is achieved through a redistribution of system load, where the dynamic load is shifted from the fuel cell to the battery. Although this means that battery throughput is increased, it reflects an intentional trade-off for long-term efficiency instead of short-term efficiency.

The research questions suggested in this thesis can be answered as follows. First, the ECMS framework can be extended to include degradation effects, via a reformulation of the existing cost function to incorporate penalty terms. Second, the resulting non-linear and non-differentiable optimization problem can be solved analytically using a piecewise formulation, while maintaining computational efficiency and compatibility for real-time implementation. Third, the proposed health-aware strategy leads to significantly reduced degradation indicators while maintaining similar energy efficiency, showing its potential.

5.2 Limitations

Despite the promising results, there are still several limitations that should be acknowledged.

First, as the proposed method is in the early stage of development, all testing and validation have been carried out in the simulation environment. Due to the simplification in the simulation model, the results may not fully represent real-world operating conditions.

Second, to simplify the cost function and facilitate the derivation of the analytical solution, a simplified battery degradation model is adopted. However, it may limit the ability to fully capture the complex aging behavior of the battery.

Finally, the proposed method incorporates a weighting factor for the battery degradation cost to balance the trade-off between fuel cell and battery degradation. For each vehicle configuration, this factor needs to be tuned to achieve optimal performance. At present, this parameter tuning work is performed manually and is time consuming.

5.3 Future work

Future work will focus on addressing the limitations mentioned before.

First, as the development progresses, the proposed method should be validated on a real vehicle to evaluate its performance. Potential issues that are not observed in the simulation environment may arise during real world operation, requiring further refinement to ensure robustness and applicability.

Second, to improve the accuracy of the degradation model, a more detailed battery degradation model can be incorporated. Consequently, a more suitable analytical solution method is required to handle the increased model complexity.

Finally, to reduce the effort and time associated with manual tuning of the weighting factor for battery degradation cost, an automated tuning method can be developed.

Bibliography

[1] A. B. M. Ali, A. K. Nemah, Y. A. Al Bahadli, and Ehsan Kianfar, “Principles and performance and types, advantages and disadvantages of fuel cells: A review,” Case Studies in Chemical and Environmental Engineering, vol. 10, p. 100920, Dec. 2024, doi: 10.1016/j.cscee.2024.100920.

[2] Y. Liu et al., “Durability experiments and performance degradation characteristics of proton exchange membrane fuel cell stack based on real vehicle road spectrum,” International Journal of Hydrogen Energy, vol. 234, p. 155082, May 2026, doi: 10.1016/j.ijhydene.2026.155082.

[3] Pollock et al., “Battery Electric Vehicles: A Study on State of Charge and Cost-Effective Solutions for Addressing Range Anxiety,” Machines, vol. 13, no. 5, p. 411, May 2025, doi: 10.3390/machines13050411.

[4] D. Pevec, J. Babic, A. Carvalho, Y. Ghiassi-Farrokhfal, W. Ketter, and V. Podobnik, “Electric Vehicle Range Anxiety: An Obstacle for the Personal Transportation (R)evolution?,” in 2019 4th International Conference on Smart and Sustainable Technologies (SpliTech), Split, Croatia: IEEE, Jun. 2019, pp. 1–8. doi: 10.23919/SpliTech.2019.8783178.

[5] J. Wang, W. Zhang, X. Luke Wen, R. Tu, and D. He, “Modeling battery electric vehicle users’ charging decisions in scenarios with both time-related and distance-related anxiety,” Travel Behaviour and Society, vol. 42, p. 101111, Jan. 2026, doi: 10.1016/j.tbs.2025.101111.

[6] Z. Bashir et al., “Next-generation thermal management systems for lithium-ion batteries: Enhancing the performance and safety in electric vehicles,” Journal of Environmental Chemical Engineering, vol. 14, no. 3, p. 122529, Jun. 2026, doi: 10.1016/j.jece.2026.122529.

[7] K. R. Ngoy et al., “Lithium-ion batteries and the future of sustainable energy: A comprehensive review,” Renewable and Sustainable Energy Reviews, vol. 223, p. 115971, Nov. 2025, doi: 10.1016/j.rser.2025.115971.

[8] N. A. A. Qasem and G. A. Q. Abdulrahman, “A Recent Comprehensive Review of Fuel Cells: History, Types, and Applications,” International Journal of Energy Research, vol. 2024, no. 1, p. 7271748, Jan. 2024, doi: 10.1155/2024/7271748.

[9] L. Fan, Z. Tu, and S. H. Chan, “Recent development of hydrogen and fuel cell technologies: A review,” Energy Reports, vol. 7, pp. 8421–8446, Nov. 2021, doi: 10.1016/j.egyr.2021.08.003.

[10] H. Weydahl, S. Møller-Holst, G. Hagen, and B. Børresen, “Transient response of a proton exchange membrane fuel cell,” Journal of Power Sources, vol. 171, no. 2, pp. 321–330, Sep. 2007, doi: 10.1016/j.jpowsour.2007.06.073.

[11] Q. Li, W. Chen, N. Zhang, Z. Luo, and B. Chen, “Dynamic response characteristics of proton exchange membrane fuel cell during transient loading: An experiment study,” International Journal of Hydrogen Energy, vol. 92, pp. 1–13, Nov. 2024, doi: 10.1016/j.ijhydene.2024.10.232.

[12] M. Yue, S. Jemei, R. Gouriveau, and N. Zerhouni, “Review on health-conscious energy management strategies for fuel cell hybrid electric vehicles: Degradation models and strategies,” International Journal of Hydrogen Energy, vol. 44, no. 13, pp. 6844–6861, Mar. 2019, doi: 10.1016/j.ijhydene.2019.01.190.

[13] A. Loskutov, A. Kurkin, A. Shalukho, I. Lipuzhin, and R. Bedretdinov, “Investigation of PEM Fuel Cell Characteristics in Steady and Dynamic Operation Modes,” Energies, vol. 15, no. 19, p. 6863, Sep. 2022, doi: 10.3390/en15196863.

[14] X. Zhao et al., “Energy management strategies for fuel cell hybrid electric vehicles: Classification, comparison, and outlook,” Energy Conversion and Management, vol. 270, p. 116179, Oct. 2022, doi: 10.1016/j.enconman.2022.116179.

[15] X. Hu, C. Zou, X. Tang, T. Liu, and L. Hu, “Cost-Optimal Energy Management of Hybrid Electric Vehicles Using Fuel Cell/Battery Health-Aware Predictive Control,” *IEEE Transactions on Power Electronics*, vol. 35, no. 1, pp. 382–392, Jan. 2020.

[16] Zhang, H. Huang, G. Zhang, Z. Dai, Y. Wen, and L. Jiang, “Cycle life studies of lithium-ion power batteries for electric vehicles: A review,” Journal of Energy Storage, vol. 93, p. 112231, Jul. 2024, doi: 10.1016/j.est.2024.112231.

[17] S. Onori, L. Serrao, and G. Rizzoni, Hybrid Electric Vehicles: Energy Management Strategies. London, U.K.: Springer, 2016, doi: 10.1007/978-1-4471-6781-5.

[18] D. Chatterjee, P. K. Biswas, C. Sain, A. Roy, and F. Ahmad, “Efficient Energy Management Strategy for Fuel Cell Hybrid Electric Vehicles Using Classifier Fusion Technique,” IEEE Access, vol. 11, pp. 97135–97146, 2023, doi: 10.1109/ACCESS.2023.3312618.

[19] X. Li, Y. Wang, D. Yang, and Z. Chen, “Adaptive energy management strategy for fuel cell/battery hybrid vehicles using Pontryagin’s Minimal Principle,” Journal of Power Sources, vol. 440, p. 227105, Nov. 2019, doi: 10.1016/j.jpowsour.2019.227105.

[20] M. Maaruf, A. Babangida, I. Ahmed, M. Khalid, and P. T. Szemes, “Advanced control strategies for fuel cell hybrid electric vehicles — A review,” Energy Conversion and Management: X, vol. 28, p. 101354, Oct. 2025, doi: 10.1016/j.ecmx.2025.101354.

[21] P. G. Anselma, “Dynamic Programming Based Rapid Energy Management of Hybrid Electric Vehicles with Constraints on Smooth Driving, Battery State-of-Charge and Battery State-of-Health,” Energies, vol. 15, no. 5, p. 1665, Feb. 2022, doi: 10.3390/en15051665.

[22] N. Sulaiman, M. A. Hannan, A. Mohamed, E. H. Majlan, and W. R. Wan Daud, “A review on energy management system for fuel cell hybrid electric vehicle: Issues and challenges,” *Renewable and Sustainable Energy Reviews*, vol. 52, pp. 802–814, Dec. 2015.

[23] M. N. Boukoberine, M. F. Zia, T. Berghout, and M. Benbouzid, “Reinforcement learning-based energy management for hybrid electric vehicles: A comprehen-

sive up-to-date review on methods, challenges, and research gaps," Energy and AI, vol. 21, p. 100514, Sep. 2025, doi: 10.1016/j.egyai.2025.100514.

[24] M. İnci, M. Büyük, M. H. Demir, and G. İlbey, "A review and research on fuel cell electric vehicles: Topologies, power electronic converters, energy management methods, technical challenges, marketing and future aspects," Renewable and Sustainable Energy Reviews, vol. 137, p. 110648, Mar. 2021, doi: 10.1016/j.rser.2020.110648.

[25] C. P. Sahwal, S. Sengupta, and T. Q. Dinh, "Advanced equivalent consumption minimization strategy for fuel cell hybrid electric vehicles," *Journal of Cleaner Production*, vol. 437, Art. no. 140366, 2024, doi: 10.1016/j.jclepro.2024.140366.

[26] C. Jia, H. He, J. Zhou, J. Li, Z. Wei, and K. Li, "Learning-based model predictive energy management for fuel cell hybrid electric bus with health-aware control," Applied Energy, vol. 355, p. 122228, Feb. 2024, doi: 10.1016/j.apenergy.2023.122228.

[27] A. Alyakhni, L. Boulon, J.-M. Vinassa, and O. Briat, "A Comprehensive Review on Energy Management Strategies for Electric Vehicles Considering Degradation Using Aging Models," *IEEE Access*, vol. 9, pp. 143922–143940, 2021, doi: 10.1109/ACCESS.2021.3120563.

[28] H. Li, A. Ravey, A. N'Diaye, and A. Djerdir, "Equivalent consumption minimization strategy for fuel cell hybrid electric vehicle considering fuel cell degradation," in *2017 IEEE Transportation Electrification Conference and Expo (ITEC)*, Chicago, IL, USA: IEEE, Jun. 2017, pp. 540–544. doi: 10.1109/ITEC.2017.7993328.

[29] P. Pei and H. Chen, "Main factors affecting the lifetime of Proton Exchange Membrane fuel cells in vehicle applications: A review," Applied Energy, vol. 125, pp. 60–75, Jul. 2014, doi: 10.1016/j.apenergy.2014.03.048.

[30] R. Han, H. He, Z. Zhang, S. Quan, and J. Chen, "A multi-objective hierarchical energy management strategy for a distributed fuel-cell hybrid electric tracked vehicle," *Journal of Energy Storage*, vol. 76, p. 109858, Jan. 2024, doi: 10.1016/j.est.2023.109858.

[31] C. Jia *et al.*, "A novel energy management strategy for hybrid electric bus with fuel cell health and battery thermal- and health-constrained awareness," *Energy*, vol. 271, p. 127105, May 2023, doi: 10.1016/j.energy.2023.127105.

DEPARTMENT OF ELECTRICAL ENGINEERING
CHALMERS UNIVERSITY OF TECHNOLOGY
Gothenburg, Sweden
www.chalmers.se

CHALMERS
UNIVERSITY OF TECHNOLOGY